Atmos. Chem. Phys., 13, 9057–9082, 2013
www.atmos-chem-phys.net/13/9057/2013/
doi:10.5194/acp-13-9057-2013

Atmospheric Chemistry and Physics Open Access

Key chemical NO_x sink uncertainties and how they influence top-down emissions of nitrogen oxides

T. Stavrakou[1], J.-F. Müller[1], K. F. Boersma[2,3], R. J. van der A[2], J. Kurokawa[4], T. Ohara[5], and Q. Zhang[6]

[1]Belgian Institute for Space Aeronomy, Avenue Circulaire 3, 1180, Brussels, Belgium
[2]Royal Netherlands Meteorological Institute (KNMI), Wilhelminalaan 10, De Bilt, the Netherlands
[3]Eindhoven University of Technology, Fluid Dynamics Lab, Eindhoven, the Netherlands
[4]Asia Center for Air Pollution Research, Niigata, Japan
[5]National Institute for Environmental Studies, Tsukuba, Ibaraki, Japan
[6]Center for Earth System Science, Tsinghua University, Beijing, China

Correspondence to: T. Stavrakou (jenny@aeronomie.be)

Received: 12 March 2013 – Published in Atmos. Chem. Phys. Discuss.: 22 March 2013
Revised: 10 July 2013 – Accepted: 30 July 2013 – Published: 10 September 2013

Abstract. Triggered by recent developments from laboratory and field studies regarding major NO_x sink pathways in the troposphere, this study evaluates the influence of chemical uncertainties in NO_x sinks for global NO_x distributions calculated by the IMAGESv2 chemistry-transport model, and quantifies their significance for top-down NO_x emission estimates. Our study focuses on five key chemical parameters believed to be of primary importance, more specifically, the rate of the reaction of NO_2 with OH radicals, the newly identified HNO_3-forming channel in the reaction of NO with HO_2, the reactive uptake of N_2O_5 and HO_2 by aerosols, and the regeneration of OH in the oxidation of isoprene. Sensitivity simulations are performed to estimate the impact of each source of uncertainty. The model calculations show that, although the NO_2+OH reaction is the largest NO_x sink globally accounting for ca. 60 % of the total sink, the reactions contributing the most to the overall uncertainty are the formation of HNO_3 in NO+HO_2, leading to NO_x column changes exceeding a factor of two over tropical regions, and the uptake of HO_2 by aqueous aerosols, in particular over East and South Asia.

Emission inversion experiments are carried out using model settings which either minimise (MINLOSS) or maximise (MAXLOSS) the total NO_x sink, both constrained by one year of OMI NO_2 column data from the DOMINO v2 KNMI algorithm. The choice of the model setup is found to have a major impact on the top-down flux estimates, with 75 % higher emissions for MAXLOSS compared to the MINLOSS inversion globally. Even larger departures are found for soil NO (factor of 2) and lightning (1.8). The global anthropogenic source is better constrained (factor of 1.57) than the natural sources, except over South Asia where the combined uncertainty primarily associated to the NO+HO_2 reaction in summer and HO_2 uptake by aerosol in winter lead to top-down emission differences exceeding a factor of 2.

Evaluation of the emission optimisation is performed against independent satellite observations from the SCIAMACHY sensor, with airborne NO_2 measurements of the INTEX-A and INTEX-B campaigns, as well as with two new bottom-up inventories of anthropogenic emissions in Asia (REASv2) and China (MEIC). Neither the MINLOSS nor the MAXLOSS setup succeeds in providing the best possible match with all independent datasets. Whereas the minimum sink assumption leads to better agreement with aircraft NO_2 profile measurements, consistent with the results of a previous analysis (Henderson et al., 2012), the same assumption leads to unrealistic features in the inferred distribution of emissions over China. Clearly, although our study addresses an important issue which was largely overlooked in previous inversion exercises, and demonstrates the strong influence of NO_x loss uncertainties on top-down emission fluxes, additional processes need to be considered which could also influence the inferred source.

Published by Copernicus Publications on behalf of the European Geosciences Union.

1 Introduction

Sources of nitrogen oxides in the atmosphere are predominantly anthropogenic. According to state-of-art estimates, anthropogenic NO_x accounts for about 65 % of the annual global NO_x flux, whereas natural emissions from fires, soils and lightning are less significant on the global scale, and are estimated at about 9 %, 17 % and 6 %, respectively (e.g. Jaeglé et al., 2005; Müller and Stavrakou, 2005). The uncertainties in these estimates are, however, significant, especially for natural sources. To narrow down these uncertainties, top-down or inverse modelling methods constrained by tropospheric NO_2 vertical column abundances observed from space have been widely used to evaluate and complement the bottom-up inventories used in atmospheric models (e.g. Müller and Stavrakou, 2005; Stavrakou et al., 2008; Zhao and Wang, 2009; Lin et al., 2010; Lin, 2012; Mijling and van der A, 2012; Miyazaki et al., 2012a).

Inverse modelling adjusts the emission fluxes used in a chemistry-transport model in order to reduce the mismatch between the predictions of the model and atmospheric observations. This is often realised iteratively by varying the emissions until the model/data biases are minimised within their assigned errors. This approach implicitly assumes that the relationship between the emission fluxes and the atmospheric abundances is reasonably well simulated by the model, so that the model/data mismatch can be mostly attributed to errors in the emission inventories. In other words, the uncertainties associated to the bottom-up emissions are assumed to be larger than errors in the model or in the measurements used to constrain the inversion. Nevertheless, a series of recent developments regarding chemical NO_x sinks and the oxidising capacity of the atmosphere (Mollner et al., 2010; Butkovskaya et al., 2007, 2009; Henderson et al., 2012; Brown et al., 2009; Lelieveld et al., 2008; Mao et al., 2013) point to flaws in the current mechanisms implemented in global models, implying potentially large impacts on simulated NO_x concentrations, and consequently on top-down NO_x emission estimates.

These developments concern firstly the main tropospheric NO_x removal channel, i.e. the reaction of NO_2 with OH radicals, forming nitric acid. It was shown in a laboratory study that its reaction rate at room temperature is lower than previously recommended (Mollner et al., 2010), and further, aircraft observations were used to show that its reaction rate in the upper troposphere was even more largely overpredicted at the low temperatures typical of the upper troposphere (Henderson et al., 2012). Secondly, a series of laboratory experiments performed by Butkovskaya et al. (2007, 2009) suggested an additional loss process for NO_x through a nitric acid formation channel in the $NO+HO_2$ reaction. Although this channel is quite minor compared to the traditional pathway forming NO_2+OH (less than 0.5 % in dry air), it has the potential to represent a significant HNO_3 formation pathway (Cariolle et al., 2008); furthermore, it was found to proceed much faster in the presence of water vapour. This could strongly affect the NO_2 concentrations, especially in the lower troposphere and in tropical regions. Thirdly, field measurements (Brown et al., 2009) suggested that reactive uptake of N_2O_5 at the surface of aerosols proceeds at rates substantially lower than predicted by parameterizations widely used in global models (e.g. Evans and Jacob, 2005; Davis et al., 2008). Finally, the hydroxyl radical (OH) levels have possibly large errors in models. For example, field campaigns point to strong underpredictions of OH levels in low-NO_x, high-isoprene environments (Lelieveld et al., 2008), for reasons still unclear (Peeters et al., 2009; Crounse et al., 2011), although simple expedients have been proposed to crudely compensate for the model underprediction (Lelieveld et al., 2008). In more polluted environments characterised by heavy aerosol loadings, the effect of HO_2 radical uptake by aqueous aerosols might be severely underestimated in models (Mao et al., 2013), leading to possibly large OH level overestimations, although field campaigns around Chinese megacities point to large OH underestimations by models (Hofzumahaus et al., 2009; Lu et al., 2013), for reasons still unclear.

A thorough discussion of the above sources of uncertainty is presented in Sect. 2, and their importance on the NO_2 abundances simulated with the IMAGESv2 global CTM is addressed in Sect. 4.

Based on the above, two model setups are designed to either minimise (MINLOSS simulation) or maximise (MAXLOSS) the NO_x sink in the model. These scenarios are meant to provide a measure of the overall uncertainty related to the major chemical NO_x losses. They do not address other sources of uncertainty, however, such as errors related to meteorological fields or other model parameters. Recently, a systematic analysis of meteorological and chemical parameters affecting the NO_x simulation over China in a CTM by Lin et al. (2012), showed that errors in meteorology affect significantly the modelled NO_2 columns, although their regionally-averaged overall reported uncertainty accounting for all parameters was lower than 20 %. Note that this estimation might be model-dependent.

The MINLOSS and MAXLOSS setups are used in an inverse modelling framework using the adjoint of the IMAGESv2 model (e.g. Müller and Stavrakou, 2005; Stavrakou et al., 2008, 2012). The inversion experiments are constrained by vertical NO_2 tropospheric columns retrieved from the Ozone Monitoring Instrument (OMI) (Boersma et al., 2011) (Sect. 3). Sensitivity calculations illustrating the effect of NO_x sink uncertainties on the distribution of NO_x sinks are presented in Sect. 4. The top-down estimates of NO_x fluxes as derived from MINLOSS and MAXLOSS inversions are compared in Sect. 5. Evaluation of the results against independent measurements and inventories is presented in Sect. 6. More specifically, the model predictions before and after inversion are compared against (i) NO_2 column data from SCIAMACHY instrument aboard ENVISAT (Sect. 6.1), and (ii) airborne NO_2 profiles from INTEX-A

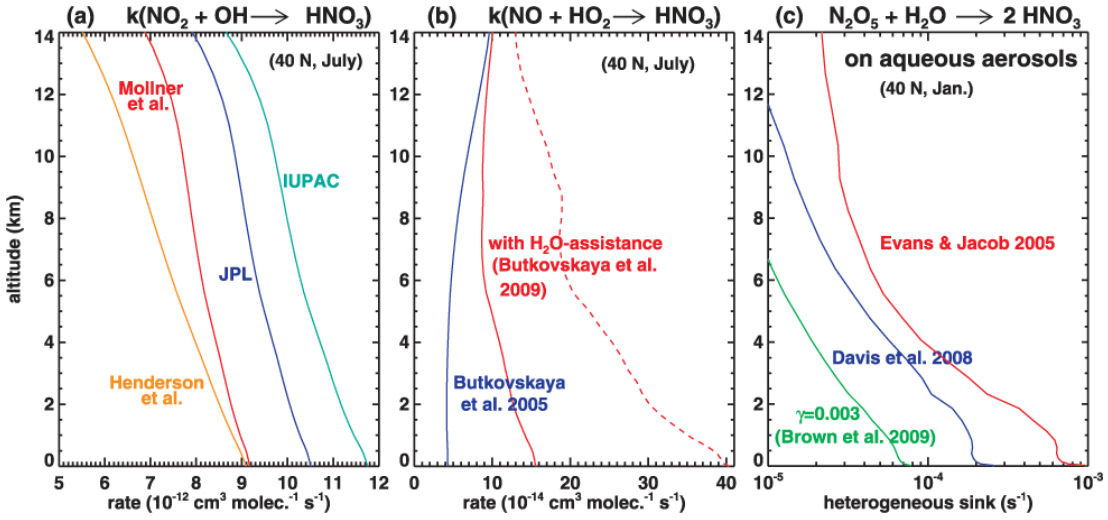

Fig. 1. Zonally averaged vertical profiles at 40° N of **(a)** the NO_2 + OH reaction rate in July, **(b)** the NO + HO_2 → HNO_3 reaction rate in July, and **(c)** the heterogeneous sink of N_2O_5 on aqueous aerosols over continents in January. The continuous red line in panel **(b)** assumes that the NO-reaction rate of the $HO_2 \cdot H_2O$ complex (k_w) is constant, whereas the dashed red line uses the temperature and pressure dependence of the rate in dry conditions (k_d).

and INTEX-B missions (Sect. 6.2). The top-down emissions are also directly compared with two state-of-the-art bottom-up emission inventories for Asia and for China (Sect. 6.3). Finally, conclusions are drawn in Sect. 7.

2 Uncertainties in NO_x sinks

2.1 The NO_2+OH → HNO_3 reaction

Despite its crucial role as the primary sink of NO_x in the troposphere, the rate constant for the termolecular association reaction, $NO_2 + OH + M \rightarrow HNO_3 + M$, has remained very difficult to measure with accuracy under atmospheric conditions. Recently, its expression has been revised by Mollner et al. (2010) based on room temperature experiments performed using improved experimental methods relying on the simultaneous measurement of all reactants and products in the reaction (Donahue, 2011). The measured rates at 298 K were significantly lower than in previous recommendations, by 23 % compared to IUPAC-2004 (Atkinson et al., 2004) and by 13 % compared to JPL (Sander et al., 2011). Since the temperature dependence of the rate was not investigated by Mollner et al. (2010), the recommendation of Sander et al. (2011) is adopted to extrapolate the experimental result of Mollner et al. (2010) at all temperatures, resulting in the following expressions for the low- and high-pressure limits of the reaction: $k_0 = 1.48 \times 10^{-30} \times (T/300)^{-3}$ cm^6 molecule^{-2} s^{-1}, and $k_{inf} = 2.58 \times 10^{-11}$ cm^3 molecule^{-1} s^{-1}.

Using upper tropospheric airborne measurements of NO_2, HNO_3, O_3, OH, and HO_2 from the Intercontinental Chemical Transport Experiment – North America (INTEX-NA) in a Bayesian modelling framework designed to constrain reaction rates, Henderson et al. (2012) found that the HNO_3 formation rate in the upper troposphere is overestimated by 22 % when adopting the rate recommendation of Sander et al. (2011). Assuming the experimental rate at 298 K by Mollner et al. (2010) to be correct, Henderson et al. (2012) deduced an updated temperature dependency: $k_0 = 1.48 \times 10^{-30} \times (T/300)^{-1.8}$ cm^6 molecule^{-2} s^{-1}.

The altitude dependence of the rate calculated using four different recommendations is displayed in Fig. 1 for mid-latitude summer conditions (left panel). Note that the IUPAC rate is overestimated in part because it represents the total NO_2 + OH + M rate constant, including the minor channel leading to pernitrous acid, HOONO. The latter channel cannot be considered a true NO_x sink, because HOONO rapidly decomposes back to NO_2 and OH in lower tropospheric conditions (Sander et al., 2011). A reasonable estimation for the uncertainty on the nitric acid-forming channel in NO_2 + OH is the difference between the expressions provided by JPL and Henderson et al. (2012). The impact of this uncertainty is explored through CTM simulations carried out following either Sander et al. (2011) or Henderson et al. (2012) (JPL and MINLOSS, cf. Table 1).

2.2 The NO + HO_2 → HNO_3 reaction

A potentially important NO_x loss process is the minor HNO_3-forming channel in the reaction of NO + HO_2 identified through laboratory observations by Butkovskaya et al. (2005). Its branching ratio, determined experimentally between 223–300 K under dry conditions, was found to strongly vary with temperature (e.g. from 0.18 % at 298 K to

Table 1. Forward simulations conducted with the global model, with the corresponding calculated contributions of each sink process to the global tropospheric sink of NO_x, the global tropospheric NO_x lifetime (diurnal average, in days), and the global lifetime of methane with respect to OH-reaction in the troposphere (in years).

Simulations	Description	NO_2+OH sink (%)	NO+HO_2 sink (%)	Aerosol sink (%)	Other sinks (%)	τ_{NO_x} (days)	$\tau^{OH}_{CH_4}$ (years)
MINLOSS	k(NO_2+OH) from Henderson et al. (2012) HNO_3 channel in NO+HO_2 ignored $\gamma_{N_2O_5}$ from Brown et al. (2009) γ_{HO_2} = 1 with $Y_{H_2O_2}$ = 0 (Mao et al., 2013) MIM2 isoprene oxidation mechanism	61.0	0	14.0	25.0	1.49	8.1
MOLLNER	as MINLOSS, k(NO_2+OH) rate constant from Mollner et al. (2010)	61.4	0	13.6	24.9	1.42	8.3
JPL	as MINLOSS, k(NO_2+OH) rate constant from Sander et al. (2011)	62.9	0	12.7	24.4	1.34	8.7
BUTKO1	as MINLOSS, including HNO_3 channel in NO+HO_2 (Butkovskaya et al., 2005)	50.2	12.2	13.4	24.2	1.26	9.2
BUTKO2	as BUTKO1, including H_2O-assistance to HNO_3 channel (Butkovskaya et al., 2009) assuming T- and p-independent k_w	44.0	26.1	13.1	24.9	1.13	10.6
BUTKO3	as BUTKO2, using T- and p-dependent k_w	26.3	43.5	9.5	20.7	0.85	14.3
DAVIS	as MINLOSS, N_2O_5 reaction probability on sulfate aerosols from Davis et al. (2008)	56.5	0	19.3	24.1	1.43	8.2
MIM2+	as MINLOSS, with the MIM2+ isoprene mechanism (Lelieveld et al., 2008)	61.3	0	14.3	24.5	1.48	8.0
HO2L	as MINLOSS, γ_{HO_2} = 0.2 with $Y_{H_2O_2}$ = 0.5	63.8	0	12.8	23.4	1.33	7.3
MAXLOSS	k(NO_2+OH) from Sander et al. (2011) NO+HO_2 $\rightarrow$$HNO_3$ (Butkovskaya et al., 2009) $\gamma_{N_2O_5}$ from Davis et al. (2008) γ_{HO_2} = 0.2 with $Y_{H_2O_2}$ = 0.5 MIM2+ isoprene oxidation mechanism	42.5	23.8	13.6	20.1	0.84	10.0

0.87 % at 223 K at 200 Torr), according to the expression

$$\beta_d = 5.3/T + 6.4 \times 10^{-6} P - 0.0173$$

(P in Torr) (Butkovskaya et al., 2005, 2007; Cariolle et al., 2008).

The overall reaction rate under dry conditions (k_d) is the product of this branching ratio by the Sander et al. (2011) recommended value for the NO + HO_2 reaction rate:

$$k_d = 3.3 \cdot 10^{-12} \exp(270/T) \cdot \beta_d.$$

Recent modelling studies have investigated the impacts of the addition of the new channel on the distribution of HNO_3, NO_x, HO_x and O_3 (Cariolle et al., 2008), on the trends of atmospheric species and radiative forcing (Søvde et al., 2011), and on the effects of aviation on atmospheric composition (Gottschaldt et al., 2013).

Further experiments showed that the HNO_3 yield is strongly enhanced in presence of water vapour (Butkovskaya et al., 2009). Assuming that this effect is due to the reaction of NO with the $HO_2 \cdot H_2O$ complex, the rate of the reaction NO + $HO_2 \cdot H_2O \rightarrow HNO_3$ was estimated under their experimental conditions (298 K, 200 Torr):

$$k_w^{exp} = 6 \times 10^{-13}\,\mathrm{cm^3\,molecule^{-1}s^{-1}}.$$

This value is equal to about 42 times the reaction rate under dry conditions at those experimental conditions. Unfortunately, the temperature and pressure dependence of this rate is unknown. The complexed fraction f_c of the hydroperoxyl radical HO_2 is estimated from the equilibrium constant of HO_2+H_2O $\leftrightarrow$ $HO_2 \cdot H_2O$:

$$f_c = \frac{1}{1 + 1/(K_{eq} \cdot [H_2O])},$$

with $K_{eq} = 2.4 \times 10^{-25} \exp(4350/T)\ cm^3\ molecule^{-1}$ (Sander et al., 2011). The overall rate of the NO + $HO_2 \rightarrow$ HNO_3 reaction in moist air is estimated using

$$k = k_d \cdot (1 - f_c) + k_w \cdot f_c.$$

Under the assumption that k_w is temperature- and pressure-independent (i.e. $k_w = k_w^{exp}$), the H_2O-assistance in the HNO_3-forming channel leads to a factor of 2–3 increase of the rate constant below 4 km (Fig.1, middle panel), whereas the gap closes at higher altitudes as air becomes drier. However, this enhancement reaches much larger values (factor of 8) if the temperature- and pressure-dependence of k_d is adopted (i.e. $k_w = 42 \cdot k_d$), as assumed in a recent modelling study (Gottschaldt et al., 2013).

The implications of the new reaction on the global modelled NO_2 columns are investigated in three simulations (BUTKO1, BUTKO2, BUTKO3) differing by their treatment of H_2O-assistance, as detailed in Table 1.

2.3 Heterogeneous reaction on sulfate aerosols

The heterogeneous hydrolysis of N_2O_5 at the surface of aerosols is an important NO_x loss process during nighttime. Its overall impact is largest in polluted environments (where aerosol loadings and N_2O_5 formation rates are high) during winter (when nights are longer and hydroxyl radical levels are at their lowest). Among different aerosol types, sulfate-containing aerosols are putatively characterised by the highest reaction probability (e.g. Evans and Jacob, 2005). Two commonly used parameterizations for the reaction probability on sulfate-containing aerosols ($\gamma_{N_2O_5}$) by Evans and Jacob (2005) and by Davis et al. (2008), are based on laboratory measurements and account for the effect of temperature and relative humidity. Davis et al. (2008) includes a dependence on aerosol (dry/wet) state and provides a further distinction between different sulfate- and nitrate-containing aerosols, including sulfuric acid, ammonium sulfate, bisulfate and nitrate. Evans and Jacob (2005) also propose recommendations for the reaction probability on organic and black carbon, dust and sea-salt. The possible influence of organics on $\gamma_{N_2O_5}$ is, however, neglected in both parameterizations.

Brown et al. (2009) determined reactive uptake coefficients for N_2O_5 using field measurements of O_3, NO_x, and aerosol surface area obtained during the night flights of the TexAQS II (Second Texas Air Quality Study) campaign in 2006. This study revealed that $\gamma_{N_2O_5}$ (i) lies in the range $0.5–6 \times 10^{-3}$, i.e. much lower than previously reported laboratory-based values, and (ii) contrary to current belief, does not exhibit a clear dependence on relative humidity or aerosol composition. The average value for the uptake coefficient derived by these measurements is equal to 0.003, by up to an order of magnitude lower than in parameterizations currently utilised in atmospheric models. Supporting evidence for the low value of the uptake coefficient is provided by direct N_2O_5 reactivity measurements on ambient aerosol particles (Bertram et al., 2009), where the observed values were found to be by a factor of ten lower compared with current parameterizations. Organic material at the aerosol surface has been identified as a candidate explanation for the reduction of the accommodation coefficient (McNeill et al., 2006).

The N_2O_5 sink rate on aerosols calculated for mid-latitude winter conditions using different parameterizations are compared in Fig. 1 (right panel). Note that the uptake coefficient on hydrophilic carbonaceous aerosols is taken to be 0.003 in all cases; for simplicity, only the uptake coefficient on sulfate/ammonium/nitrate aerosol has been varied. Overall, the Brown et al. (2009) value leads to a sink lower by a factor of 2–3 compared to the Davis et al. (2008) parameterization, and by an order of magnitude compared to Evans and Jacob (2005). To evaluate the impact of these differences on the NO_x budget and distribution, we contrast the results of two simulations, one using a constant value of 0.003 for the uptake coefficient, as suggested by Brown et al. (2009), and one using the Davis et al. (2008) parameterization (MINLOSS and DAVIS simulations, respectively).

2.4 Other losses

In addition to the previous pathways of NO_x removal, the following processes are also considered.

- Dry deposition of NO_2

  The dry deposition of NO_2 to vegetation and soils is a direct NO_x sink, computed with the resistance-in-series scheme of Wesely (1989).

- Wet and dry deposition of organic nitrates

  NO_x is converted to organic nitrate through reactions of NO_3 with alkenes, as well as through reactions of peroxy radicals with NO and acyl peroxy radicals with NO_2. Organic nitrates are temporary NO_x reservoirs with lifetimes of the order of minutes to weeks which can be transported away from the source regions, where they can either release NO_2 through decomposition or oxidation, or undergo wet and/or dry deposition. Besides peroxy acyl nitrates (PANs), isoprene and monoterpene nitrates are believed to represent the largest contribution to the total organic nitrate budget (Beaver et al., 2012; Browne and Cohen, 2012). Their precise yields and fate remain poorly understood despite recent advances regarding the further oxidation of nitrates produced in the OH- and NO_3- oxidation of isoprene (Paulot et al., 2009; Kwan et al., 2012). Their role is relatively limited in IMAGESv2 due to their short lifetimes and their oversimplified reaction scheme which follows the MIM2 mechanism (Taraborrelli et al., 2009). In itself, nitrate formation and export should not be considered a NO_x sink, even though it might significantly deplete NO_x levels in the formation region (Paulot et al., 2012). Therefore, only the

deposition of organic nitrate will be considered a NO_x sink in this study.

– Reaction of NO_3 with aldehydes and with dimethylsulfide $(CH_3)_2S$

  NO_3 can be converted to nitric acid by reaction with aldehydes, $NO_3 + RCHO \rightarrow HNO_3 + RCO\cdot$, or by reaction with dimethylsulfide, $NO_3 + (CH_3)_2S \rightarrow HNO_3 + CH_3SCH_2$. Whereas the reaction with aldehydes is only a minor sink in our model calculations, the reaction with $(CH_3)_2S$ is significant above oceans.

According to our model calculations, the sum of the above sinks represents only a small part (ca. 20 %) of the global tropospheric NO_x sink (Table 1). Uncertainties related to these sinks will not be addressed in this study, although they might be substantial. As a result, the overall NO_x sink uncertainty derived in this study should only be seen as a lower limit. In particular, a more detailed treatment of organic nitrate chemistry could result in increased NO_x sinks in regions influenced by biogenic isoprene emissions.

2.5 OH radical concentration

An additional source of uncertainty resides in the abundances of OH radicals, responsible for the conversion of NO_2 to nitric acid as well as for the removal of most reactive compounds in the troposphere. We discuss briefly below three possibly major reasons for this uncertainty, namely, the degradation chemistry of isoprene, the production of HONO, whose photolysis provides a direct OH source, and the heterogeneous HO_2 loss on aerosols.

There is strong evidence from field campaigns in mid-latitude forests, tropical forests and other rural environments (e.g. Lelieveld et al., 2008; Ren et al., 2008; Hofzumahaus et al., 2009) that OH levels are largely underestimated in models when using traditional isoprene chemical chemistry (Butler et al., 2008; Kubistin et al., 2010; Stone et al., 2011). Furthermore, the model underprediction is found to increase for increasing isoprene concentrations as well as for decreasing NO levels (Lu et al., 2013). Although the causes of this behaviour are still under heated debate, they imply the existence of OH recycling processes counteracting the OH suppression due to reaction with isoprene and its degradation products. Lelieveld et al. (2008) suggested that between 2 and 4 OH radicals are formed in the reaction of isoprene peroxy radicals with HO_2 as implemented in the MIM2 chemical mechanism (Taraborrelli et al., 2009). Although this approach allowed to better align the model to the data, it was not supported by theoretical or experimental evidence. A substantial progress towards the elucidation of the high observed OH concentrations was provided by the theoretical studies of Peeters et al. (2009) and Peeters and Müller (2010), proposing that the isomerization of specific isoprene peroxy radicals leads to substantial HO_x regeneration. Tested in global models (e.g. Stavrakou et al., 2010), the mechanism was found to be very efficient in enhancing HO_x concentrations in the boundary layer, providing good agreement with available data. However, several open issues merit further investigation, e.g. the subsequent degradation chemistry of the isomerization products, as well as the reconciliation of theoretical findings with experimental evidence from the laboratory (Crounse et al., 2011).

The second source of uncertainty in OH levels originates in the primary OH radical source through HONO photolysis, which has been identified from field observations as quite significant in the lower troposphere, especially in the early morning (e.g. Elshorbany et al., 2009). A strong missing source of HONO has been invoked by recent studies to reconcile the large discrepancies found between observed and modelled HONO abundances during daytime (Sörgel et al., 2011; Su et al., 2011). The formation processes leading to these unexpectedly enhanced HONO concentrations are still under investigation, like nitrate photolysis following HNO_3 deposition on forest canopy surfaces (Zhou et al., 2011), heterogeneous conversion of NO_2 on ground and aerosol surfaces (Su et al., 2008), or HONO release from soil nitrites (Su et al., 2011). However, evidence favouring one or the other process is still partial, and therefore, the atmospheric impact of HONO, in particular its contribution to the production of OH radicals, remains an open issue.

Finally, the reactive uptake of HO_2 by aerosols is a potentially important yet very uncertain HO_x sink. This reaction is generally assumed to form H_2O_2 with a yield ($Y_{H_2O_2}$) equal to 0.5, and a reaction probability (γ_{HO_2}) value of 0.2 has been recommended for use in atmospheric models (Jacob, 2000). Laboratory measurements at atmospherically-relevant conditions revealed that the uptake coefficients for dry $(NH_4)_2SO_4$ and NaCl aerosol were lower than 0.05, whereas for wet aerosols, measured γ_{HO_2} ranged between ca. 0.1 and 0.2 (Taketani et al., 2008). Much lower values (< 0.01) by more than an order of magnitude over both dry and wet aerosols were derived in a recent laboratory study (Matthews et al., 2012), possibly reflecting a saturation effect. On the other hand, values higher than 0.2 were observed in the presence of transition metal ions, most notably copper, in aqueous aerosols (Cooper and Abbatt, 1996; Taketani et al., 2008; Matthews et al., 2012). Furthermore, the presence of iron favours pathways leading ultimately to H_2O (i.e. $Y_{H_2O_2} = 0$) instead of H_2O_2 (Mao et al., 2013), thereby increasing the overall HO_x depleting effect of aerosols. Under molar concentrations of copper and iron typically found in fine aerosols in the United States and in other (moderately) polluted areas, Mao et al. (2013) estimated using a detailed aerosol model that the reactive uptake coefficient of HO_2 should be close to unity, with H_2O as main reaction product. This result was found to be consistent with HO_x measurements in field studies in various environments. Its impact on the global tropospheric composition was calculated using a global CTM and found to be substantial (Mao et al., 2013), although the adopted assumptions ($\gamma_{HO_2} = 1$ and $Y_{H_2O_2} = 0$

on all aerosol types) clearly represent an exaggeration, since the HO_2 uptake cannot be expected to be efficient on dry aerosols, and since laboratory determinations of γ_{HO_2} indicate values significantly lower than unity even for Cu-doped aerosols. Nevertheless, this efficient uptake scenario is also adopted in our baseline simulation (MINLOSS), except that only fine mode aqueous aerosols (i.e. hydrophilic carbonaceous and sulfate/ammonium/nitrate aerosols) are allowed to promote the HO_2 uptake. Neglecting the effect of coarse mode aerosols should not lead to large errors, since sulfate and organic aerosols largely dominate the aerosol loading and therefore the aerosol surface area over most continental areas, especially over NO_x source regions (Jimenez et al., 2009).

In order to test the uncertainties related to isoprene chemistry, we performed a sensitivity simulation denoted MIM2+ (Table 1), which includes the recycling mechanism proposed by Lelieveld et al. (2008). The OH production from HONO is not considered in the current version of the model. We test the sensitivity of the model with respect to uncertainties in HO_2 aerosol uptake by carrying out a simulation where γ_{HO_2} is set to a lower value (0.2), and $Y_{H_2O_2}$ is set equal to 0.5 (HO2L run of Table 1).

3 Satellite-driven source inversion of NO_x sources

3.1 Tropospheric NO_2 columns from OMI

OMI (Ozone Monitoring Instrument) is a Dutch-Finnish nadir viewing imaging spectrometer flying on a sun-synchronous orbit crossing the local equator at ca. 13:40 LT (Levelt et al., 2006). Launched aboard the Aura platform in 2004, OMI measures in the UV-visible spectral window (270–500 nm) at a nadir resolution of 13×24 km. The Dutch OMI tropospheric NO_2 version 2 (DOMINO v2) data product (Boersma et al., 2011), publicly available through the TEMIS portal (http://www.temis.nl), is used in this study. This version constitutes a major improvement compared to the previous DOMINO v1 tropospheric NO_2 columns (Boersma et al., 2011). DOMINO v2 has been used thus far in assimilation studies (Miyazaki et al., 2012a, b), air quality assessments (McLinden et al., 2012), as well as for validation purposes (Irie et al., 2012; Ma et al., 2013).

DOMINO v2 tropospheric NO_2 columns are reduced by 20 % in winter, and by 10 % in summer over polluted regions, compared to the DOMINO v1 product. Larger discrepancies between DOMINO v2 and v1 occur, however, on regional scales. Cloudy pixels (i.e. with cloud fraction > 0.2) and pixels affected by the so-called row anomaly (i.e. track positions 53–54, since June 2007) were excluded. The OMI tropospheric NO_2 retrieval error for individual, cloud-free pixels comprises the uncertainties on the slant and on the stratospheric slant column, estimated at 0.7×10^{15} and 0.15×10^{15} molec. cm^{-2}, respectively, and the uncertainty on the tropospheric AMF, lying between 10 and 40 % (Boersma et al., 2007). The total error of the DOMINO v2 product is estimated to be lower, from 1.0×10^{15} molec. cm^{-2} + 30 % for v1, to 1.0×10^{15} molec. cm^{-2} + 25 % for DOMINO v2 (Boersma et al., 2011).

3.2 NO_2 simulated by IMAGESv2 CTM

The IMAGESv2 global chemistry-transport model simulates the concentrations of 132 trace species at a resolution of $2° \times 2.5°$, and at 40 sigma-pressure levels between the Earth's surface and the lower stratosphere (44 hPa). As a drawback of the global model domain, its relatively coarse resolution should be acknowledged as a possible source of error in NO_2 abundances and sensitivities, given the non-linear character of tropospheric chemistry. The model includes the chemistry of 22 precursor NMVOCs, as detailed in the Supplement. Meteorological fields are obtained from ERA-Interim analyses of the European Center of Medium-Range Weather Forecasts (ECMWF) for the year of the simulation (2007). Convection follows the parameterization of Costen et al. (1988) constrained by ERA-Interim updraft mass fluxes. Turbulent mixing in the planetary boundary layer (PBL) is parameterized as vertical diffusion (Müller and Brasseur, 1995) based on ERA-Interim boundary layer heights. Details about the model, including its evaluation against radionuclide data (^{222}Rn and ^{85}Kr), airborne and satellite measurements, and other CTMs can be found in previously published work (e.g. Müller and Brasseur, 1995; Müller and Stavrakou, 2005; van Noije et al., 2006; Stavrakou et al., 2008, 2012). The chemistry is solved by the fourth order Rosenbrock solver of the Kinetic Preprocessor software tool (KPP, Sandu et al., 2006). The model time step for the forward simulations is taken equal to 4 h. Note that the chemical solver uses an adaptable internal timestep, which is often much shorter than the external timestep of 4 h. As described in more detail in Stavrakou et al. (2009a), the effects of diurnal variations are accounted for through correction factors calculated from a detailed model run with a 20 min time step, which is also used to estimate the NO_2 column diurnal shape profile. This diurnal cycle simulation accounts for diurnal variations in the photolysis and kinetic rates, in the meteorological fields, and in the emissions.

The model uses anthropogenic emissions of NO_x, CO, SO_2 and NH_3 from the EDGAR 3.2 FT2000 inventory for year 2000 (http://themasites.pbl.nl/tridion/en/themasites/edgar/), overwritten by the REAS version 1 (Ohara et al., 2007) inventory over Asia, and EMEP emissions over Europe (http://www.ceip.at/). Over the US, the EDGAR emission is scaled to the National Emission Inventory (NEI, http://www.epa.gov/ttn/chief/eiinformation.html) values for each year. Anthropogenic emissions of NMVOCs (ethane, propane, ethene, propene, acetylene, methanol, benzene, toluene, xylenes, formic and acetic acids, and the sum of other NMVOCs) are provided by the RETRO inventory for

year 2000 (Schultz et al., 2007) overwritten by REASv1 over Asia.

The seasonality of anthropogenic emissions accounts for (i) a temperature dependence of vehicle emissions from the MOBILE 6 algorithm (Giannelli et al., 2002), and (ii) the seasonal variation of residential heating. In MOBILE 6, the effect of cold starts on CO road transport emissions is accounted for by a correction factor applied for temperatures lower than 18 °C, equal to $1 + (18 - T_C) \cdot 0.05$, with T_C the temperature in Celsius. Road emissions of NO_x are only slightly temperature-dependent, a correction factor equal to $1 + (24 - T_C) \cdot 0.0072$ being applied only for temperatures above 24 °C. The sectoral split of anthropogenic emissions is obtained from EDGAR. The seasonal variation of heating emissions is estimated by assuming that these emissions are proportional to the number of heating degree-days, with a threshold of 18 °C.

Diurnal and weekly profiles of CO, NO_x and VOC anthropogenic emissions for OECD countries are obtained from Jenkin et al. (2000). A diurnal cycle is also applied to biomass burning emissions (Stavrakou et al., 2009a) as well as to lightning emissions, assumed to follow the diurnal cycle of convective updraft fluxes.

For the year 2007, global annual anthropogenic NO_x emissions (excluding ship and aircraft emissions) are estimated at 25.7 Tg N. Emissions from ships and aircraft contribute to an additional 4.2 Tg N in 2007.

Open vegetation fires are obtained from the Global Fire Emission Database (GFEDv3, van der Werf et al., 2010) and amount to 4.3 Tg N globally in 2007. The horizontal distribution of lightning NO emissions (scaled at $3\,\mathrm{Tg\,N\,yr^{-1}}$ globally) combines a spaceborne climatology (LIS/OTD) for the number of flashes with a parameterization (Price and Rind, 1993; Martin et al., 2007) which uses cloud top heights and convective precipitation rates from ECMWF. The lightning emissions are vertically distributed according to Pickering et al. (1998).

Soil emissions are calculated according to the algorithm of Yienger and Levy (1995). Biome data are taken from the compilation of Matthews (1983) (http://data.giss.nasa.gov/landuse/vegeem.html), and cropland distribution from the land use database of Klagenfurt University (Erb et al., 2007). Total fertilizer consumption per year and per country is obtained from the International Fertilizer Association (IFA, http://www.fertilizer.org), and the fraction of fertilizer consumption which is used in rice paddies is obtained from the Food and Agriculture Organization (FAO, http://faostat.fao.org). The fraction of the applied fertilizer assumed to be lost as NO is equal to 1 % for all crops (Steinkamp and Lawrence, 2011), except for rice paddies where it is assumed to be zero (Yienger and Levy, 1995). The total soil emission is scaled to 8 Tg N globally.

Inorganic (i.e. sulfate/ammonium/nitrate/water) aerosols are calculated using EQSAM (Metzger et al., 2002). The calculation of organic aerosols (OA) and black carbon (BC) follows Stavrakou et al. (2012). Since, however, the model using unadjusted POA anthropogenic emissions (Bond et al., 2004) and SOA parameterization (Ceulemans et al., 2012) largely underestimates organic carbon (OC) measurements over polluted areas, an additional OA source is included, of magnitude equal to three times the POA source over the United States, and five times the POA source in other regions. Moreover, the parameterized SOA production due to monoterpene oxidation in low-NO_x conditions is reduced by a factor of 5 in order to provide a better match with observations in biogenically-influenced regions. Although crude, this adjustment strongly reduces the biases with the measurements, as detailed in the Supplement. Previous model-based analyses (Spracklen et al., 2011; Heald et al., 2011) have pointed to the existence of a large OA source over anthropogenically-influenced regions, of the order of $100\,\mathrm{Tg\,yr^{-1}}$. The precise nature of the additional source is currently unclear, although SOA very likely makes up for a large fraction of it (Yuan et al., 2013). The additional source included in IMAGESv2 amounts to 68 Tg(OA) per year, whereas the global SOA source amounts to $53\,\mathrm{Tg\,yr^{-1}}$, primarily due to biogenic emissions. More details on the treatment of inorganic and carbonaceous aerosols in IMAGESv2 is provided in the Supplement.

The wet removal scheme for gases and aerosols (Stavrakou et al., 2009c) is based on ECMWF analyses for cloud fraction, cloud ice and liquid/mixed water content, convective and stratiform precipitation data.

Nine forward global simulations are performed (Table 1) to evaluate the sensitivity of the calculated NO_2 column and NO_x lifetime to the NO_x sink uncertainties described in Sect. 2. The simulations are performed for year 2007, and the model is initialized on 1 September 2006 (cf. Sect. 3.3).

The simulated monthly averaged NO_2 columns are compared to the corresponding DOMINO v2 averages binned at the horizontal resolution of the model. The monthly averages are calculated from daily values accounting for the number of measurements and averaging kernel for each day (also binned onto the model resolution) and for the sampling times of observation at each location.

The errors associated to the monthly DOMINO v2 averages are estimated from the reported retrieval errors, following a super-observation approach as in Eskes et al. (2003). The super-observations are the measurement averages at the model resolution. The super-observation errors account for an assumed error correlation of 50 % between retrieval errors on individual measurements contributing to the same super-observation. The total monthly error combines this super-observation retrieval error and an assumed model/representativity error of 0.5×10^{15} molec. $\mathrm{cm^{-2}}$.

3.3 The inversion setup

The discrete adjoint of the IMAGESv2 model is used to infer top-down NO_x emission estimates constrained by

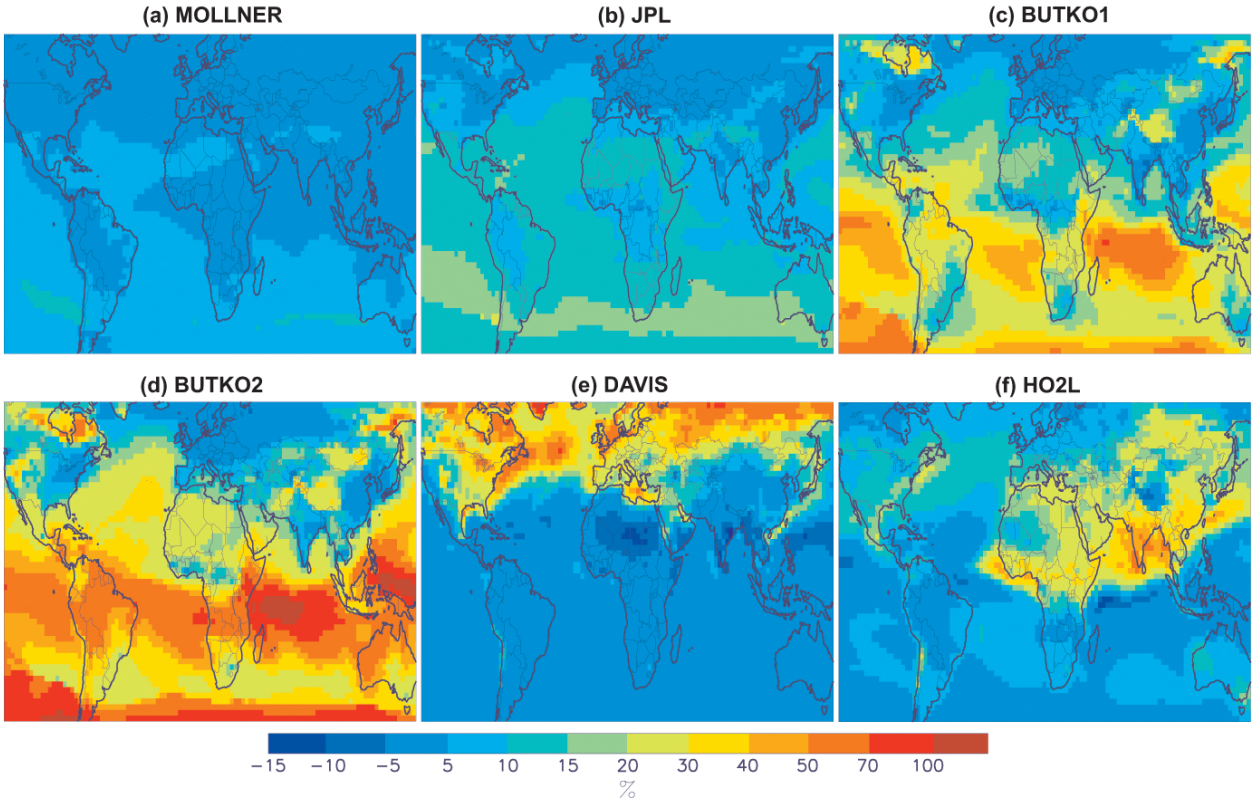

Fig. 2. Percentage difference in the sink rate of the tropospheric NO_x column between the simulations of Table 1 and the base run MINLOSS ((RUN-MINLOSS)/MINLOSS)*100, for January 2007.

OMI columns. This method, described in previous work (Stavrakou et al., 2006, 2008), allows for deriving monthly emission estimates at the resolution of the model ($2° \times 2.5°$) for each of the NO_x emitting categories (anthropogenic, biomass burning, soil and lightning). The assumed error on the anthropogenic emissions by country is set equal to a factor of 1.6 and 2 for OECD and other countries, respectively, to a factor of 2 for soil emissions, and 2.5 for vegetation burning and lightning.

Two optimizations are carried out, which use NO_x sink assumptions of either the MINLOSS and MAXLOSS simulations (Table 1). They are performed at $2° \times 2.5°$ model resolution and use one year (2007) of OMI NO_2 global columns as constraints. The total number of control variables to be optimized in these source inversions is approximately equal to 70 000.

4 Importance of uncertainties in NO_x losses addressed with IMAGESv2

Using MINLOSS as our baseline run, the influence of the chemical uncertainties discussed in Sect. 2 is illustrated by their impact on the sink rate of the tropospheric NO_x column in January and July (Figs. 2 and 3). Note that for simplicity, the results given in this section concern the daily averaged sink rate of the tropospheric column calculated without averaging kernels; in some cases, however, the sensitivity of the sink rate in the hours preceding the satellite overpass time and weighted by the altitude-dependent instrument sensitivity might differ markedly from the sensitivity shown here. This is most evident in the case of the sink due to N_2O_5 uptake by aerosols, which is primarily a nighttime process.

By far the largest impact on the sink rate is the change due to the HNO_3 forming channel in the reaction $NO+HO_2$, especially when H_2O-assistance is included (BUTKO1-3). The impact reaches up to a factor of two over tropical oceans, as a result of the high abundance in HO_2 and water vapour in these regions (Fig. 2d). Over polluted regions, the relative impact of this loss process is found to be lower, due to the predominance of other sinks ($OH+NO_2$ in summer and $N_2O_5+H_2O$ in winter) in those regions. Overall, the relative contribution of this reaction to the global tropospheric NO_x sink amounts to 12 % in the case of BUTKO1 scenario, and reaches 26–43 % when water-assistance is taken into account (BUTKO2-3). As a result, the global NO_x lifetime is reduced by 18, 32 and 75 % in BUTKO1, BUTKO2 and BUTKO3, respectively, compared to the base run, whereas the lifetime of methane due to reaction with OH in the troposphere (8.1 yr in MINLOSS) is increased to 9.2, 10.6 and 14.3 yr (i.e. by

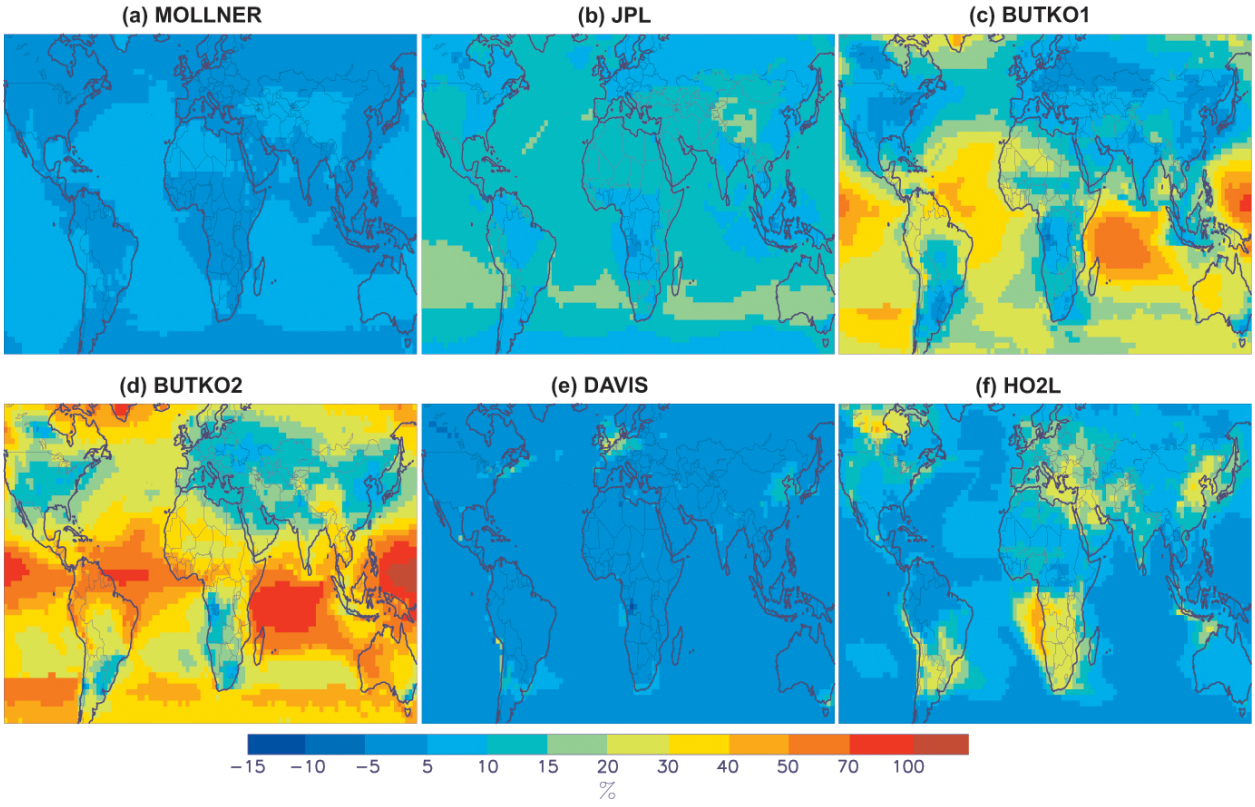

Fig. 3. Same as Fig. 2 for July 2007.

14, 31 and 76 %), respectively. These results imply a very large uncertainty associated to the temperature and pressure dependence of the rate k_w in humid conditions. The methane lifetime changes are slightly larger than the lifetime increases (11 % and 50 % without and with H_2O-assistance, respectively) estimated in the modelling study of Gottschaldt et al. (2013) which adopted the same T- and p-dependence of k_w as in our BUTKO3 simulation. Part of the discrepancy with that study might be due to the lower equilibrium constant for the complexation of HO_2 adopted by Gottschaldt et al. (2013).

Including the new channel in the HO_2+NO reaction results in an overall decrease of NO_2 columns by up to 45 % (60 %) at remote oceanic regions, and by 15 % (30 %) over the continental Tropics in BUTKO1 (BUTKO2) cases, whereas the decrease over polluted continental regions is less important (ca. 15 % in the US in BUTKO2). Note that the instrument averaging kernels and satellite overpass time are taken into account in the calculated NO_2 columns. Over Eastern China, the calculated NO_2 column changes in July in the BUTKO3 case (20–40 %) are only slightly lower than the corresponding changes (20–50 %) calculated by Lin et al. (2012) when assuming a 5 % HNO_3 yield in the HO_2+NO reaction. This good agreement reflects the HNO_3 yield in the BUTKO3 case, reaching 5 % near the surface at mid-latitudes, even though it decreases to much lower values (about 2 %) in the upper troposphere (Fig. 1).

As expected, and in qualitative agreement with Lin et al. (2012), the impact of the additional sink is largest for chemically aged air masses, far away from the emission regions. Calculated changes in the surface NO_2 mixing ratios generally do not exceed 15 % over continents in the BUTKO2 simulation. As an effect of the lower NO_x abundances, O_3 production is reduced by 4–6 % at mid-latitudes near the surface, and by up to 16 % at remote environments to southward of 50° S in the BUTKO1 run, in very good agreement with the changes reported by Cariolle et al. (2008). The enhanced NO_x sink in BUTKO2 run leads to more pronounced decreases of model surface O_3, by 5–10 % in mid-latitudes and by 20–25 % over oceans in the Southern Hemisphere.

The replacement of the low value for $\gamma_{N_2O_5}$ (0.003) by the Davis et al. (2008) parameterization for the uptake of N_2O_5 on inorganic aerosols (DAVIS simulation) leads to substantial increases in the loss rate of the NO_x column in the northern extratropical latitudes during winter. This is attributed to the low wintertime HO_x levels and to high NO_x and aerosol sources in these regions. The enhancement of the sink rate reaches 70 % in these regions in January. Note that the increased NO_x sink e.g. over Europe leads to decreased NO_x levels over neighbouring areas (e.g. Northern Africa) and therefore to decreased OH levels, explaining the decreased NO_x sink rate in those areas. Over Northern China, the very low effect of N_2O_5 uptake is explained by dry and

cold conditions causing inorganic aerosols (dominated by ammonium sulfate and ammonium nitrate) to be predominantly solid in the model in this region. The heterogeneous uptake is believed to be very slow on dry particles (Davis et al., 2008). A comparatively stronger sensitivity to N_2O_5 uptake was calculated by Lin et al. (2012), with NO_2 column changes exceeding 10 % when decreasing the uptake coefficient by a factor of 10. This is explained by the fact that the reduction was applied by Lin et al. (2012) to all aerosol types, i.e. not just to inorganic aerosols as in the DAVIS simulation. Furthermore, the parameterization of Evans and Jacob (2005) used in the reference run by Lin et al. (2012) does not account for the suppression of $\gamma_{N_2O_5}$ on dry particles.

In July, the importance of the N_2O_5 sink on aerosol is low due to the dominance of the NO_2+OH sink (Figs. 2, 3e). The sensitivity is weak in the Tropics. Globally, the N_2O_5 sink on (both inorganic and carbonaceous) aerosol, which accounts for 14 % of the sink in the baseline simulation, is increased to 19.3 % in the DAVIS case, and is responsible for a reduction of the global NO_x lifetime by 4 % (Table 1). This weak sensitivity is due to the importance of organic aerosols, which contribute significantly to the total N_2O_5 uptake, in spite of the low assumed $\gamma_{N_2O_5}$. Note that the contribution of N_2O_5 uptake on inorganic aerosols is increased from 4.2 % in MINLOSS to 10.6 % in DAVIS.

The reaction of NO_2 with OH constitutes the major loss of NO_x in the troposphere. The use of the JPL recommendation for its rate constant (JPL run) leads to increased NO_x loss rate by about 10–15 % in most areas, and by up to 20 % over the remote Southern Ocean (Table 1, Figs. 2, 3). This appears consistent with the 15–20 % difference in the rate constants in the boundary layer (Fig. 1), given that this reaction represents ca. 60 % of the total NO_x sink.

The calculated changes are comparatively lower when the Mollner et al. (2010) rate constant is used (generally < 10 %) (MOLLNER). This is explained by the fact that the rate constant adopted in the MINLOSS and MOLLNER cases are very similar in the boundary layer (Fig. 1), where most of the NO_2 column resides. Globally, the calculated NO_x lifetime is found to decrease by 5 % and 11 % in the MOLLNER and JPL simulation, respectively.

The effect of the model changes in the MIM2+ simulation is found to be small. The increased OH concentrations over low-NO_x forested areas lead to increased NO_x loss rates. The sink increase amounts to less than 1 % on the global scale, although it can reach 20 % in low-NO_x, isoprene-rich regions.

Finally, the model using a less efficient HO_x loss ($\gamma_{HO_2} = 0.2$ and $Y_{H_2O_2} = 0.5$) due to HO_2 uptake by aerosols (HO2L simulation) exhibits a strong sensitivity in regions with high aerosol concentrations, in particular over East and South Asia as well as over biomass burning areas such as Africa in the winter hemisphere and Central Canada during summer (Fig. 2–3f). In fact, HO_2 uptake appears to be the largest source of uncertainty over much of Europe and the Northeastern US in July, as well as over China in both seasons, where the NO_x sink rate is increased by up to 30 % (up to 50 % in January) when HO_2 uptake is assumed to be less efficient. Those changes are primarily due to the strong impact of the reaction on OH levels, as shown by the 11 % decrease in mass-weighted tropospheric OH concentration in the HO2L run, very similar to the 12 % change in tropospheric OH reported by Mao et al. (2013) between simulations either ignoring HO_2 uptake or adopting the same efficient uptake scenario ($\gamma_{HO_2} = 1$ and $Y_{H_2O_2} = 0$) as in MINLOSS. Annually averaged OH and HO_2 concentrations are increased by factors of up to 2 and 3, respectively, over both China and India; those changes over China are lower than in the modelling study of Mao et al. (2013), as expected since HO_2 was allowed to react on all aerosol types in the latter study, irrespective of the aerosol state. In contrast, the calculated changes over India are much lower in Mao et al. (2013), presumably due to lower organic aerosol loadings in GEOS-Chem compared with IMAGESv2. The NO_2 column changes calculated in IMAGESv2 over China are larger in January (20–35 %) compared to July (between 10 % in Southern China and almost 20 % in Northern China), in qualitative agreement with Lin et al. (2012) where the impact of a reduction of $\gamma_{N_2O_5}$ from 0.2 to 0.05 was estimated.

As seen from this analysis, the base run MINLOSS realises the lowest NO_x loss rates and the largest global tropospheric NO_x lifetime among the sensitivity tests. The MAXLOSS scenario is designed by adopting the choices which maximise the NO_x loss. This is realised by using the JPL recommendation for the NO_2+OH reaction rate, by including the HNO_3 forming channel in NO+HO_2, based on Butkovskaya et al. (2009) (with T- and p-independent k_w), $\gamma_{N_2O_5}$ on sulfate aerosols from Davis et al. (2008), $\gamma_{HO_2} = 0.2$ on aqueous aerosols (with $Y_{H_2O_2} = 0.5$), and the MIM2+ chemistry. The combination of these settings causes a strong reduction of the global NO_x lifetime, by a factor of 1.8 with respect to MINLOSS (Table 1). Note that other model uncertainties could affect the modelled NO_x columns, e.g. in meteorological parameters, in the emissions of other compounds (e.g. NMVOCs) or in chemical parameters other than those considered in this study (Lin et al., 2012). The comparison of our MINLOSS and MAXLOSS simulations should, nevertheless, provide a measure of the uncertainties associated to the major chemical NO_x pathways. The analysis of Lin et al. (2012) suggests that the uncertainties due to other factors are generally much lower than overall uncertainty considered in this study.

The daily averaged NO_x lifetimes calculated for MINLOSS and MAXLOSS cases are shown in Fig. 4 and the contribution of the main individual NO_x sinks to the total sink is illustrated in Fig. 5 for MAXLOSS. Lifetimes of less than one day are calculated in the case of MAXLOSS over most continental regions, especially in summertime and in high-NO_x environments, due to the dominance of the loss via OH. In essence, the distribution of the NO_2+OH sink reflects mainly the boundary layer OH concentration field

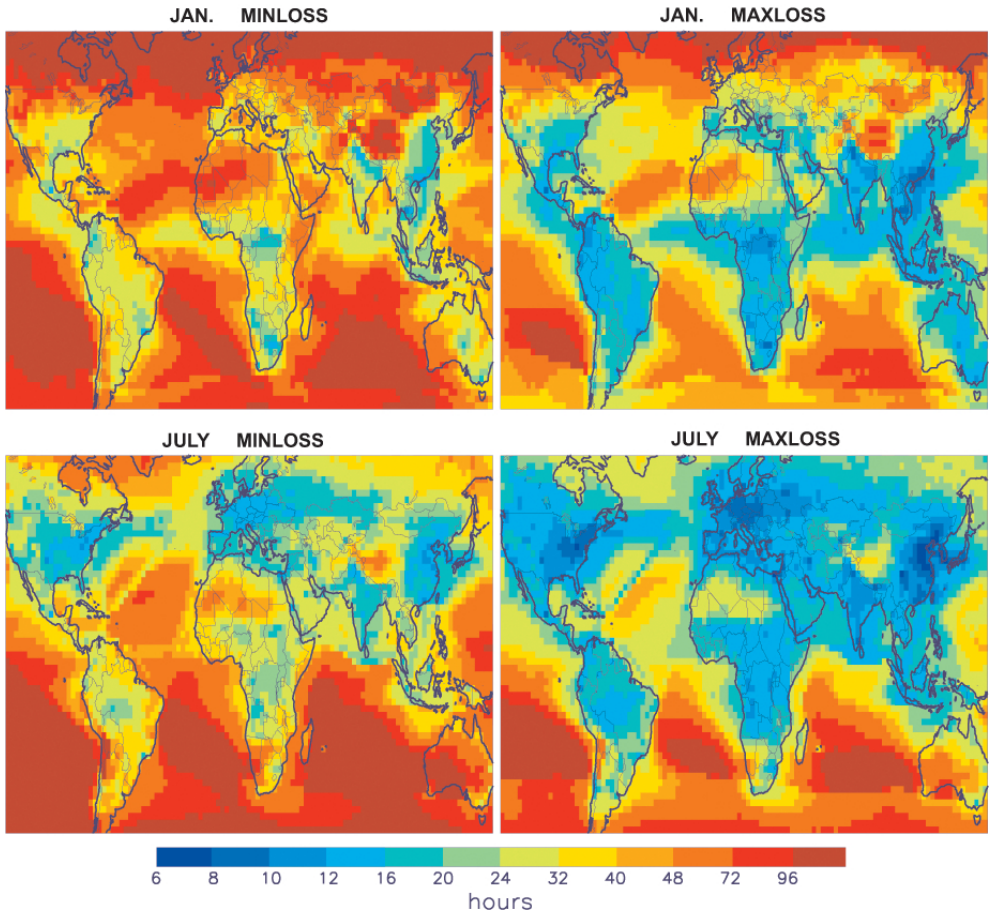

Fig. 4. Comparison of NO_x lifetimes calculated in the MINLOSS and MAXLOSS simulations in January and July 2007.

pattern (Fig. 5). The loss via NO+HO_2 occurs mostly over tropical regions, and is, on average, roughly two times lower than the loss due to NO_2+OH. In January, N_2O_5 uptake by aerosols is significant in regions with high aerosol concentrations and long nights, and is estimated to be three times more important than in July at the global scale (Fig. 5). Over oceans and high-latitude regions the lifetime can reach several days due to lower OH and NO_2 levels.

5 Top-down NO_x emissions

This section focuses on the results of the two emission inversions constrained by 2007 OMI data performed using either the MINLOSS or the MAXLOSS model settings (Table 1). The a priori and optimized tropospheric NO_x budget is summarised in Table 2, and the annual total NO_x emission update is shown in Fig. 6.

The differences between the emissions inferred by both inversions are found to be substantial, with the total NO_x source being 75 % higher in MAXLOSS compared to MINLOSS. The top-down estimates, 38 Tg N from MINLOSS against 68 Tg N from MAXLOSS, correspond to a slight decrease of the source (15 %) in the former case, and a substantial increase by 50 % in the latter, with respect to the a priori source. The annual total NO_x emission update, i.e. the ratio of a posteriori to the a priori emissions (Fig. 6), is found to be generally lower than one at mid-latitudes in MINLOSS. In tropical regions, the emissions are increased by up to a factor of two, mainly due to increased natural sources. Similar patterns are found in the case of MAXLOSS, but with much higher emission updates, generally between 1 and 2 over polluted regions, and between 2 and 5 in the Tropics.

In a relative sense, the largest discrepancies between the two inversions concern natural emissions. Global NO_x emissions from lightning and soil differ by 80 % and 125 % between MAXLOSS and MINLOSS, respectively. This is the consequence of the large difference in NO_x lifetimes between the two inversions in tropical regions (Fig. 4). This difference is further amplified by chemical feedbacks. In most tropospheric conditions, a NO_x emission increase leads to an increase in OH (through the HO_2+NO→OH+NO_2 reaction) and therefore in the NO_x sink rate. In the context of inverse modelling, this implies that larger emission increments are required in order to match the observations, to compensate

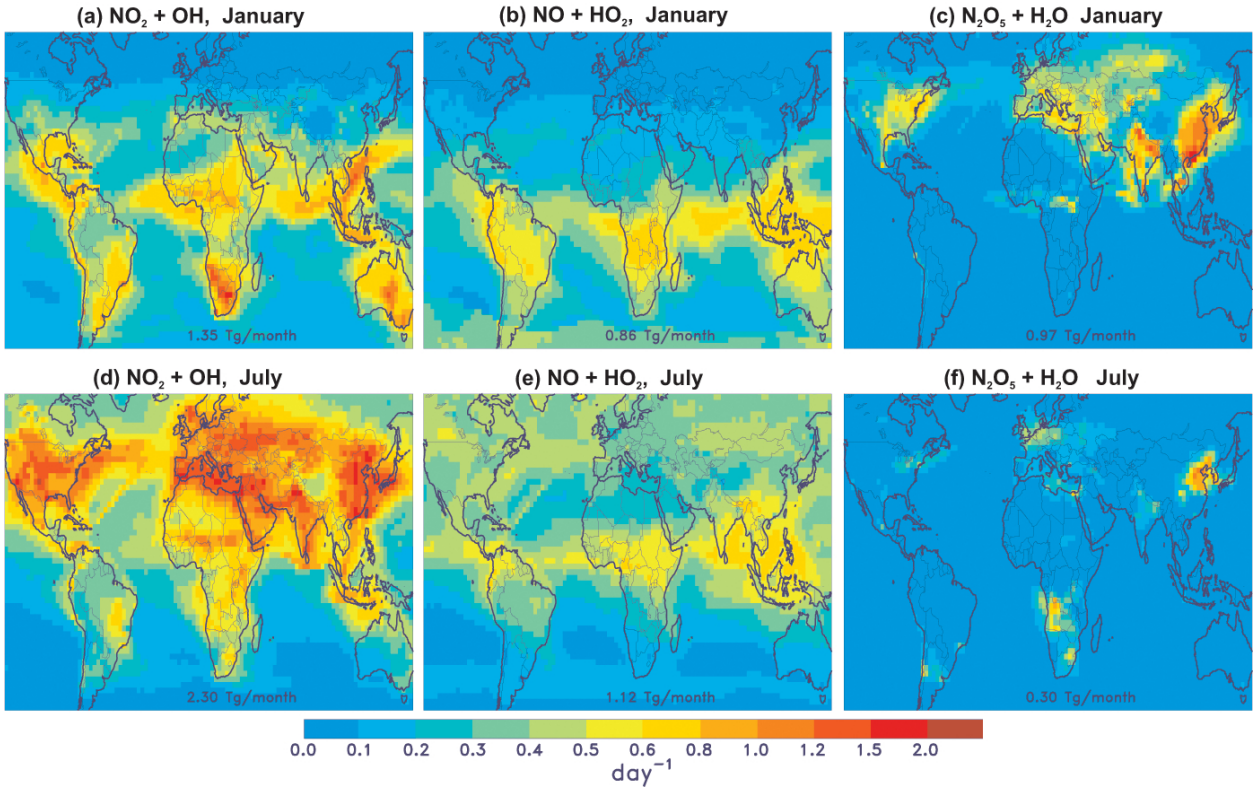

Fig. 5. Calculated contribution of **(a, d)** NO_2+OH reaction, **(b, e)** the HNO_3-forming channel in NO+HO_2 reaction, and **(c, f)** the heterogeneous N_2O_5 sink to the tropospheric NO_x sink rate (day^{-1}) in January **(a–c)** and July **(d–f)** for the MAXLOSS simulation.

for this negative chemical feedback, compared to an emission inversion neglecting feedbacks. Since the NO_x emission increments are larger in MAXLOSS compared to MINLOSS, the NO_x lifetime decreases (relative to the a priori) are also larger in MAXLOSS compared to MINLOSS, which amplifies the differences between the emission increments in MAXLOSS and MINLOSS.

In comparison to most global inversion studies, soil NO emission is found to be generally underestimated by the algorithm of Yienger and Levy (1995). Top-down studies derived estimates for the global soil NO source ranging between 8.9 Tg N (Jaeglé et al., 2005) and 10–12 Tg N (Müller and Stavrakou, 2005; Stavrakou et al., 2008). More recently, improvements upon the algorithm of Yienger and Levy (1995) resulted in new parameterizations yielding global above-soil NO_x emission of 10.7 Tg N (Hudman et al., 2012), and an above-canopy soil NO_x source at 8.6 Tg N (Steinkamp and Lawrence, 2011), in better agreement with satellite-derived fluxes. In the latter study, which was based on a compilation of a large number (ca. 600) of flux measurements, the emission factors for the different ecosystems were estimated from the geometrically averaged observed fluxes. However, the use of an alternative, equally plausible averaging method (the plain arithmetic average) resulted in an annual estimate of 27.6 Tg N, much higher than all previous values. This finding underscores the high uncertainty of this source, whereas the wide range of our OMI-derived estimates for soil emissions, 9–20 Tg N per year (Table 2), could be regarded as a (probably conservative) top-down uncertainty range for this source.

The global NO_x production from lightning derived in this study is estimated at 3.3–5.9 Tg N yr^{-1}, i.e. 10–100 % higher than the a priori source, with the strongest increases predicted in the Tropics. This result is in line with previously reported top-down values, ranging between 1.1 and 6.4 annually (Müller and Stavrakou, 2005; Stavrakou et al., 2008; Boersma et al., 2005). Recently, Murray et al. (2012), based on satellite lightning data, estimated a global annual source of 6 ± 0.5 Tg N, in agreement with the best estimate of 6 Tg N by Martin et al. (2007) derived through comparisons of satellite observations of NO_2, O_3 and nitric acid with a global CTM, and with the study by Schumann and Huntrieser (2007) reporting a range of 2–8 Tg N per year, based on a literature review suggesting that a thunderstorm flash produces $15(2–40) \times 10^{25}$ molecules NO per flash on average. However, this result was contradicted by a more recent study (Beirle et al., 2010) using SCIAMACHY NO_2 columns, which suggested that the production efficiency is of the order of 2×10^{25} molecules NO per flash, at the low end of the range derived by Schumann and Huntrieser (2007).

Table 2. Annual NO_x emissions and tropospheric sinks (Tg N) in the MINLOSS and MAXLOSS scenarios. Global anthropogenic includes shipping and aircraft. The total source given between brackets includes the production due to HNO_3 photolysis and reaction with OH. Regional anthropogenic emissions are italicized.

	MINLOSS		MAXLOSS	
Sources	Prior	Optimized	Prior	Optimized
Anthropogenic	29.8	22.3	29.8	35.1
Asia	*11.5*	*7.7*	*11.5*	*14.6*
Europe	*4.7*	*2.9*	*4.7*	*4.9*
N. America	*6.0*	*4.7*	*6.0*	*7.1*
China	*4.8*	*3.8*	*4.8*	*6.0*
Fires	4.3	3.7	4.3	6.7
Soil	8.0	9.0	8.0	20.4
Lightning	3.0	3.3	3.0	5.9
Total source	45.1	38.3	45.1	68.1
	(50.9)	(43.7)	(50.8)	(78.1)
Sinks				
NO_2+OH	28.3	25.0	20.6	35.1
NO+HO_2	0.0	0.0	11.3	15.1
N_2O_5+H_2O on aerosols	9.6	7.0	8.4	12.4
Other	13.1	12.0	10.5	15.7
Total sink	51.0	44.0	50.7	78.3

This lower estimate for NO production efficiency translates to an annual lightning NO_x source of 1 Tg N.

The biomass burning source is also highly sensitive to the NO_x sink scenario: global annual emissions are found to be 3.7 Tg N in MINLOSS and 6.7 Tg N in MAXLOSS, compared to 4.3 Tg N in GFEDv3. The strongest emission increments are derived over Southern Africa (factor of 2–3 in MAXLOSS) and Oceania, whereas fire emissions in South America are either close to the prior (in MAXLOSS) or significantly lower in MINLOSS). Support for higher NO_x emissions from fires is provided by an independent global database of fire emissions (Fire Inventory from NCAR, Wiedinmyer et al., 2011), where the global 2007 emissions are estimated at 6.7 Tg N.

The differences in anthropogenic global totals inferred by the inversions are significant, 22.3 Tg N in MINLOSS vs. 35.1 Tg N in MAXLOSS (cf. Table 2). Pronounced differences are also derived on the continental scale, as illustrated in Table 2. In most regions, the posterior emissions are lower than the a priori in the MINLOSS inversion, but higher when the maximum loss scenario is considered. Over China, the anthropogenic emission total is 3.8 Tg N in MINLOSS, by a factor 1.6 lower than in MAXLOSS (6 Tg yr^{-1}). The latter total is close to the 2006 top-down anthropogenic flux estimate derived from SCIAMACHY NO_2 columns, 6.3 Tg N yr^{-1} (Stavrakou et al., 2008), and is slightly lower than reported in a recent inversion study for East China (101.25–126.25° E, 19–46° N), 7.1 Tg N yr^{-1}, also constrained by DOMINO v2 NO_2 columns (Lin, 2012). Based on a bottom-up methodology for China, Zhang et al. (2007) estimated the anthropogenic emission in 2004 at 5.7 Tg N yr^{-1}. Extrapolating this value based on the emission growth rate derived by Zhang et al. (2007) between 1995–2004 (6.1 % yr^{-1}) would result in an emission estimate of 6.8 Tg N in 2007, close to the MAXLOSS result. Two recently available bottom-up inventories, namely, the latest version of the Regional Emission inventory in ASia (REAS version 2) and the Multi-resolution Emission Inventory in China (MEIC) will be compared with the OMI-derived emissions in Sect. 6.3.

The flux estimates for North America and Europe depend strongly on the inversion setup. In North America, they are found to be lower (4.7 Tg N) or higher (7.1 Tg N) in comparison with the a priori (6 Tg N) in MINLOSS and MAXLOSS, respectively, whereas the previous top-down estimate for the same region in 2006 by Stavrakou et al. (2008) lies within the above range, and is very close to the a priori (6.1 Tg N yr^{-1}). In Europe, based on data assimilation of DOMINO v2 NO_2 columns, Miyazaki et al. (2012a) reported an anthropogenic annual flux equal to 4.6 Tg N, close to our a priori value.

South Asia is the region where NO_x sink uncertainties have the largest impact: the anthropogenic emission total according to MAXLOSS (6.3 Tg N yr^{-1}) is a factor of 2.4 larger than in MINLOSS. Over India, the difference even exceeds a factor 3. This strong discrepancy over India is primarily due to the new channel in NO+HO_2 (in summer) and even more to the uptake of HO_2 by aerosols (in winter), as seen from the calculated sensitivity of NO_x sink rates to those processes (Figs. 2–3). Note that, although the uptake of N_2O_5 by aerosol is a large contribution to the daily averaged NO_x sink over East and South Asia in January (Fig. 5), it has little influence on top-down emissions because OMI samples NO_2 columns in the early afternoon. The emission update over India is highest (> 3) in January (Fig. 7), when the effect of HO_2 uptake is strongest due to high aerosol loadings and relatively slow photochemistry.

The global sources and sinks of NO_x are summarised in Table 2. Note that the direct NO_x sources are not exactly balanced by the sinks due to the conversion of HNO_3 back to NO_x totaling > 5 Tg N yr^{-1} in the troposphere. The calculated global photochemical lifetime of tropospheric HNO_3 ranges between 23 and 27 days, depending on the simulation. About 55 % of the photochemical sink is due to photolysis, the rest being due to reaction with OH.

The percentage differences between inferred total NO_x emissions in simulations MINLOSS and MAXLOSS (Fig. 7)

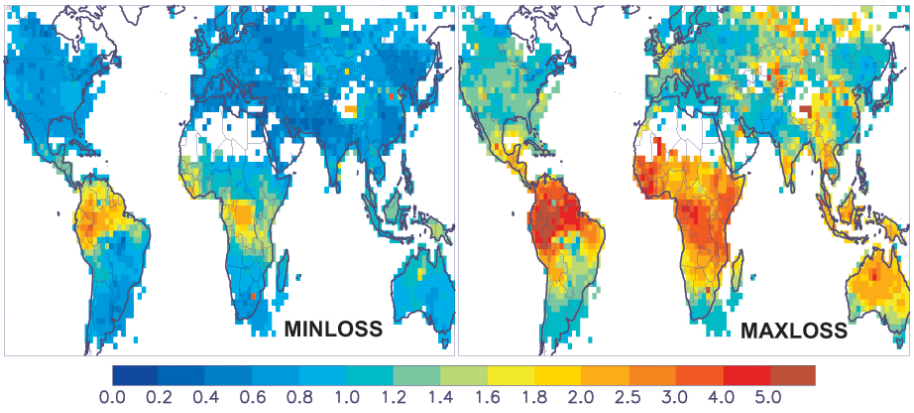

Fig. 6. Annual total NO_x emission update (optimized/a priori) inferred from inversion MINLOSS (left) and MAXLOSS (right).

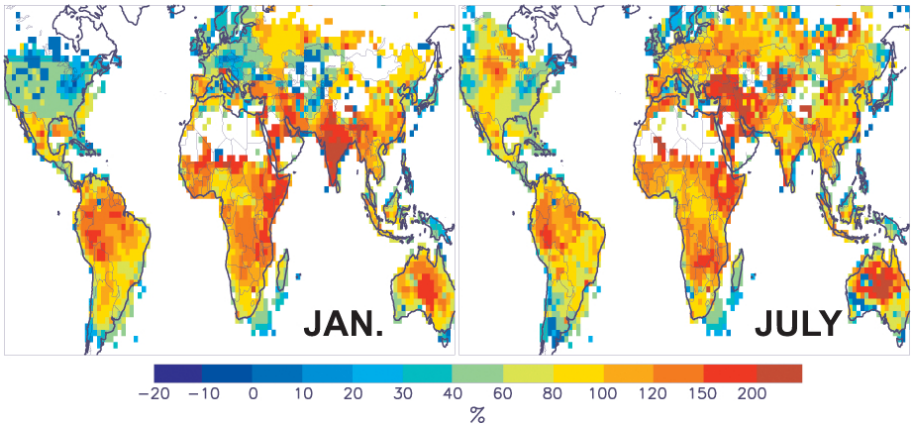

Fig. 7. Percentage difference between inferred total NO_x emission in simulations MINLOSS and MAXLOSS for January and July 2007.

are less pronounced over Europe and North America in January (generally less than 30 %) than in July (40–100 %). This relatively weak sensitivity of winter fluxes is partly explained by the longer NO_x lifetimes and increased role played by transport in determining NO_x columns over emission regions in winter. Furthermore, the winter losses are dominated by the uptake of N_2O_5 on aerosols (Fig. 5) which has only a modest influence on NO_x columns at the overpass time of OMI (13:40 LT).

Both inversions are found to modify the seasonality of anthropogenic emissions over China (Fig. 8), improving the agreement with the bottom-up inventory of Zhang et al. (2007). The December-to-July emission ratio, equal to 1.33 in MINLOSS is close to the ratio reported in Zhang et al. (2007) (1.26). However, the weaker seasonal dependence of the emissions in MAXLOSS (ratio of 1.13) agrees well with the more recent inventories (cf. Sect. 6.3). In North America and Europe, the inversions keep the main seasonality features of the a priori almost unchanged. The February peak of the a priori seasonality, due to the low temperatures and the heating-degree day approach applied to the residential emissions, is consistent with the satellite observations, especially in the MINLOSS inversion.

6 Comparisons with independent observations and inventories

6.1 SCIAMACHY NO_2 vertical columns

We evaluate the modelled a priori and a posteriori NO_2 columns against NO_2 column abundances retrieved from the SCIAMACHY UV-visible nadir sounder crossing the local equator at ca. 10h00 local time. SCIAMACHY has a ground pixel of $30 \times 60\,km^2$ and achieves global coverage within six days. For these comparisons we use SCIAMACHYv2 data distributed via the TEMIS website (www.temis.nl, Boersma et al., 2004). This product is reprocessed using the same basic algorithm for satellite observations used for DOMINO v2. Comparisons above selected regions between SCIAMACHY and modelled NO_2 columns before and after inversion and columns from OMI and SCIAMACHY are illustrated in Figs. 9 and 10.

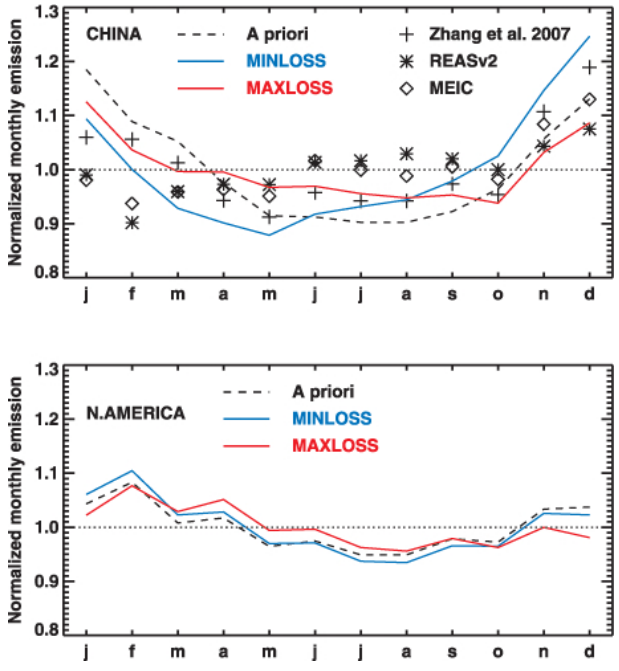

Fig. 8. Normalised seasonal variation of anthropogenic emissions over China (top) and North America (bottom).

Overall, the model/OMI data discrepancy is efficiently reduced after the optimization. Whereas relatively small changes are inferred in summer over Northern China, the column increases are more substantial in wintertime (up to factor of two in MAXLOSS), despite the reduced seasonality of anthropogenic emissions (Fig. 8). As discussed in Stavrakou et al. (2008), different photochemical regimes in summer and in winter lead to different responses of the NO_x lifetime to an emission increase, primarily because OH levels increase with NO_x in summer (due to the HO_2+NO reaction), resulting in a negative feedback, whereas the opposite effect prevails in winter (due to OH+NO_2). The role of N_2O_5 is limited because it operates only at night, as noted above.

The bias between the model and the SCIAMACHY data is significantly reduced in the a posteriori solution in Northern China, despite remaining underestimations during winter, especially in the MINLOSS case. In Western Europe and Eastern US, the optimized columns are still lower than OMI (up to 25 %), but in good agreement with SCIAMACHY data, although the MAXLOSS inversion leads to an overestimation of the columns over Europe in summertime. In Southeast Asia, the a priori columns capture quite well the seasonal pattern of the observed columns from OMI and SCIAMACHY, but their magnitudes are strongly different due to the importance of the NO+HO_2 sink in the Tropics in the MAXLOSS case. After inversion, the match between the modelled and OMI columns is excellent, however, a systematic model overprediction persists with respect to SCIAMACHY data. This overestimation is also found over tropical America and tropical Africa. It might be related to biases in the satellite products or, for example, in the diurnal cycle of emissions and/or oxidants in the model.

6.2 Aircraft campaign measurements

Modelled NO_2 profile shapes before and after inversion are evaluated against the two Intercontinental Chemical Transport Experiments INTEX-A and INTEX-B. The INTEX-A field mission (Singh et al., 2006) was undertaken between 1 July to 15 August 2004 over North America (http://www-air.larc.nasa.gov/missions/intexna/intexna.htm) The NO_2 profiles obtained in this mission are described in Singh et al. (2007). The INTEX-B two-phase mission (Singh et al., 2009) was conducted in spring 2006 (1 March–15 May) over Mexico area in March and over the Pacific in April and May (http://www.espo.nasa.gov/intex-b/).

Over North America (Fig. 11), the a priori NO_2 model profiles are quite similar with slight differences (less than 20 %) in the continental boundary layer. Both inversions succeed in reducing the bias with the observations in summertime. In spring, the MAXLOSS inversion results lead to large overestimations in the boundary layer. Over oceans (Fig. 12), the changes inferred by the inversions are small in all cases. Although biased high, the MINLOSS profiles lie closer to the measurements, especially over the North Pacific. The assumed strong sink in the MAXLOSS setup leads to significant NO_2 underestimation over all oceanic regions, especially in the mid- and upper troposphere.

6.3 Comparison with REASv2 and MEIC emission inventories

Figure 13 compares the annual inversion results from MINLOSS and MAXLOSS with the latest version of the Regional Emission inventory in ASia (REAS version 2) and the Multi-resolution Emission Inventory in China (MEIC) for the year 2007. The a priori inventory used for Asia is REASv1, except for the seasonality which has been calculated as described in Sect. 3.2.

REASv2 was developed recently by updating the REASv1 database, which was a first historical anthropogenic emission inventory in Asia covering the period from 1995 to 2003, whose major emission sources are fuel combustion, industrial process, and agricultural activities. The new REAS inventory includes most of major air pollutants and greenhouse gases: SO_2, NO_x, CO, NMVOC, PM_{10}, $PM_{2.5}$, BC, OC, NH_3, CH_4, N_2O, and CO_2. Target years are from 2000 to 2008 and areas are expanded from East, Southeast and South Asia of REASv1 to Central Asia and Asian part of Russia (Ural, West and East Siberia, and Far East). Emissions are estimated on a monthly basis for each country and region and are allocated to grids at a $0.25° \times 0.25°$ resolution. Both spatial and temporal resolutions are finer than in REASv1. Activity data such as energy consumption and

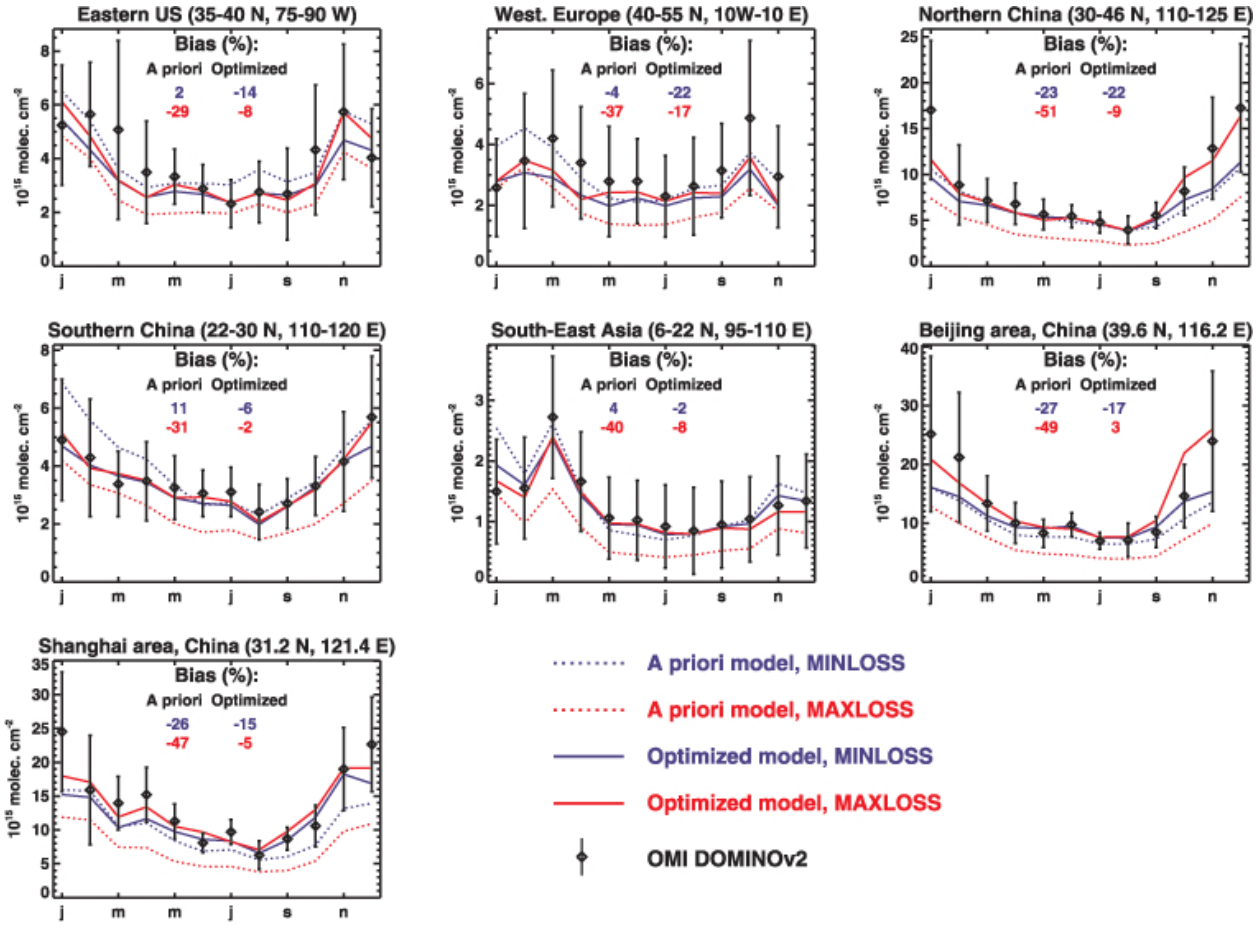

Fig. 9. Seasonal variation of NO_2 columns over large regions. Comparisons between OMI retrievals (diamonds), a priori (dotted), and optimized (solid) columns in MINLOSS (blue) and MAXLOSS (red) for 2007. Percentage biases are given inset. The NO_2 column errors are as described in Sect. 3.2.

industrial production were obtained from new statistics and database of power plants as point sources are fully updated. Country- and region-specific parameters such as emission factors and removal efficiencies were also updated by surveying recently published literature for Asian emission inventories. As for Japan, South Korea, and Taiwan, inventories of other research works based on detailed activity data and information were used in REASv2 (Kurokawa et al., 2013).

MEIC is based on a dynamic, technology-based methodology to estimate anthropogenic emission fluxes in China beyond 1990 and until the present date. Emissions are estimated for all anthropogenic sources for ten chemical species: SO_2, NO_x, CO, NMVOC, NH_3, CO_2, PM_{10}, $PM_{2.5}$, BC, and OC. Total NMVOC emissions are further speciated into species for five chemical mechanisms: CBIV, CB05, RADM2, SAPRC99, and SAPRC07. MEIC updates and improves upon the inventories developed by the same group (Zhang et al., 2007, 2009; Lei et al., 2011a). The major improvements of MEIC inventory include unit based emission inventory for power plants (Wang et al., 2012) and cement plants (Lei et al., 2011b), updates of recent activity data and emission factors from literature, and an on-line emission process database (http://www.meicmodel.org). Emissions are available for four aggregated sectors, namely, power generation, industry, residential and transportation, with monthly temporal variation and 0.25° spatial resolution.

The REASv2 and MEIC distributions are very similar both geographically and temporally over China. At the resolution of the CTM ($2° \times 2.5°$), REASv2 and MEIC are highly correlated ($r = 0.96$). Only the MAXLOSS optimization brings the model total emissions closer to REASv2 and MEIC: 6.0 Tg N yr^{-1} vs. 7.2 and 7.6 Tg N yr^{-1} in REASv2 and MEIC, respectively, whereas the MINLOSS value is only 3.8 Tg N yr^{-1}. In terms of seasonal variation (Fig. 8), both optimizations increase the share of summertime emissions and reduce the January–March normalised emissions, in better agreement with the bottom-up estimates. Although MINLOSS achieved the best match with the seasonality of Zhang et al. (2007), the seasonality of MAXLOSS emissions is in better agreement with the more recent inventories. The ratio

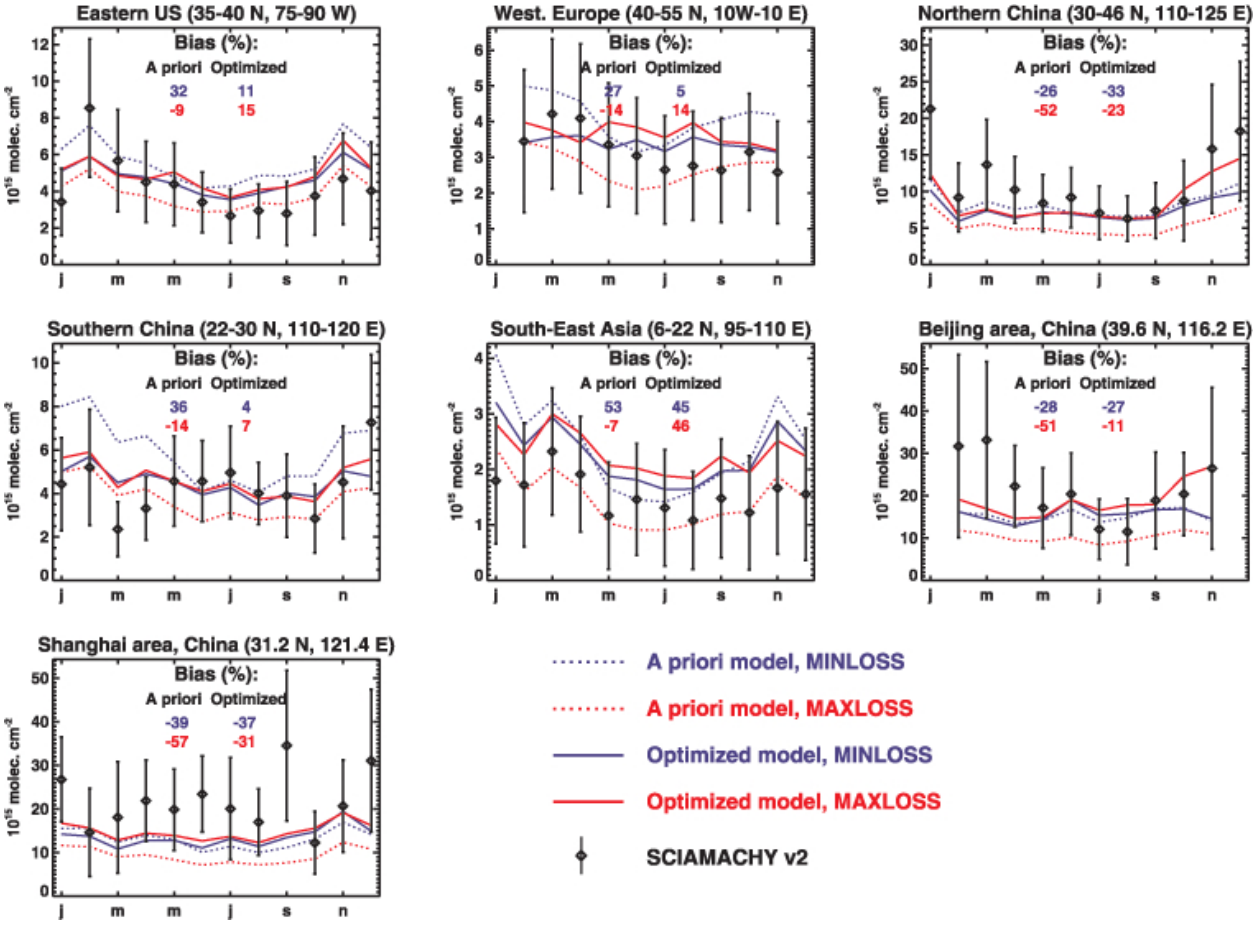

Fig. 10. Same as Fig. 9 but using SCIAMACHYv2 NO_2 retrievals and modelled columns calculated at the SCIAMACHY overpass time (10:00 LT). The NO_2 column errors are estimated using the same algorithm as for DOMINO v2.

of December to July emissions, 1.13 in MAXLOSS, agrees very well with the values derived from REASv2 (1.06) and MEIC (1.13). The a priori seasonality (too high in late winter, and too low in summer) is therefore not supported by the satellite observations.

Regarding the spatial distributions of the emissions (Fig. 13), the MINLOSS inversion leads to an emission enhancement in the North China Plain, and to emission decreases in other regions, leading to a deterioration of the correlation with the MEIC and REASv2 inventories (Table 3). The MAXLOSS inversion realises a better match with the recent inventories, as seen by the reduced root-mean-square deviations shown in Table 3.

Table 3. Spatiotemporal correlations and root-mean-square deviations, expressed in 10^{10} molec. cm^{-2} s^{-1}, of monthly NO_x emissions over China.

Correlation	A priori	MINLOSS	MAXLOSS
REASv2	0.916	0.748	0.923
MEIC	0.914	0.805	0.927
RMSD	**A priori**	**MINLOSS**	**MAXLOSS**
REASv2	8.7	12.3	6.6
MEIC	11.1	12.8	7.7

7 Conclusions

We have investigated the influence of major uncertainties in NO_x chemical sinks on the NO_x columns simulated with the IMAGESv2 model and on the top-down NO_x emission strengths derived by inverse modelling. Uncertainties in five key processes were addressed, namely, (i) the rate of the reaction $NO_2+OH \rightarrow HNO_3$, (ii) the formation of HNO_3 in the reaction $NO+HO_2$ as proposed by Butkovskaya et al. (2007, 2009), (iii) the N_2O_5 uptake by aerosols, (iv) the regeneration of OH radicals in isoprene oxidation, and (v) the uptake of HO_2 by aerosols. Through sensitivity model studies, we have shown that these uncertainties imply significant differences in the predicted NO_x columns and lifetimes:

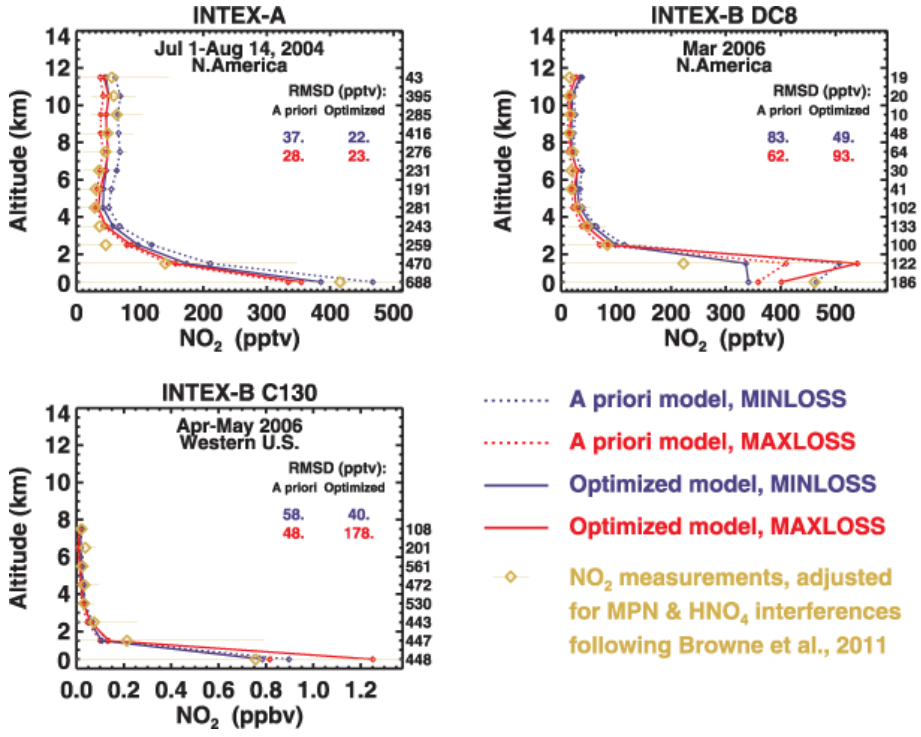

Fig. 11. A priori and optimized modelled NO_2 mixing ratios compared with observed mean mixing ratios during the INTEX-A and INTEX-B missions over North America. Note that the real measurement altitudes are taken into account when deriving the model averages. Observed NO_2 mixing ratios are adjusted for methyl peroxy nitrate (MPN) and HNO_4 interferences according to Browne et al. (2011).

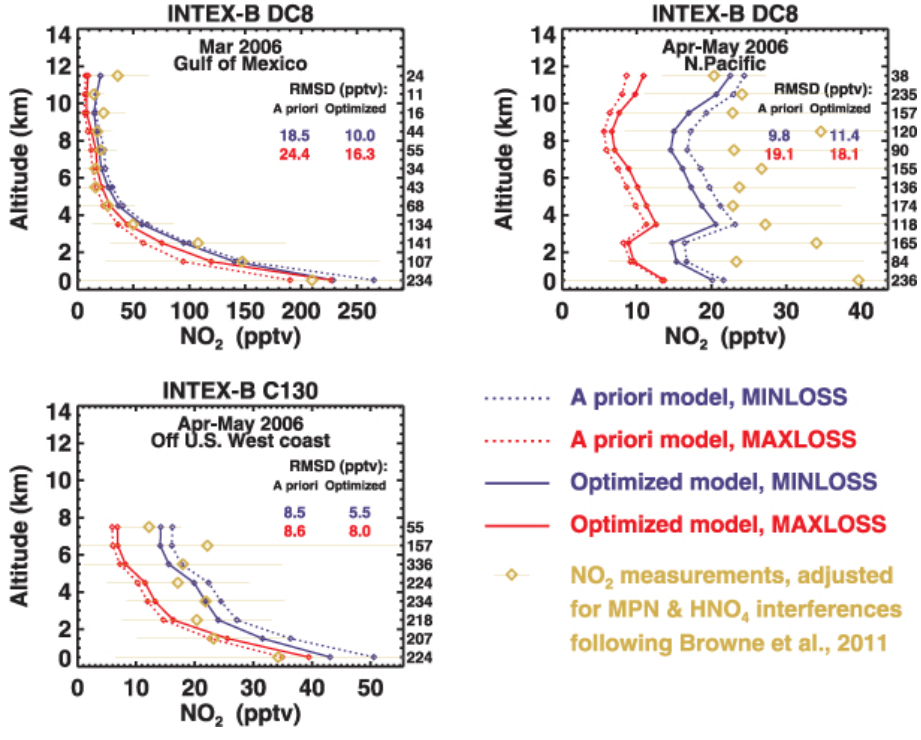

Fig. 12. Same as Fig. 11 but for oceanic areas.

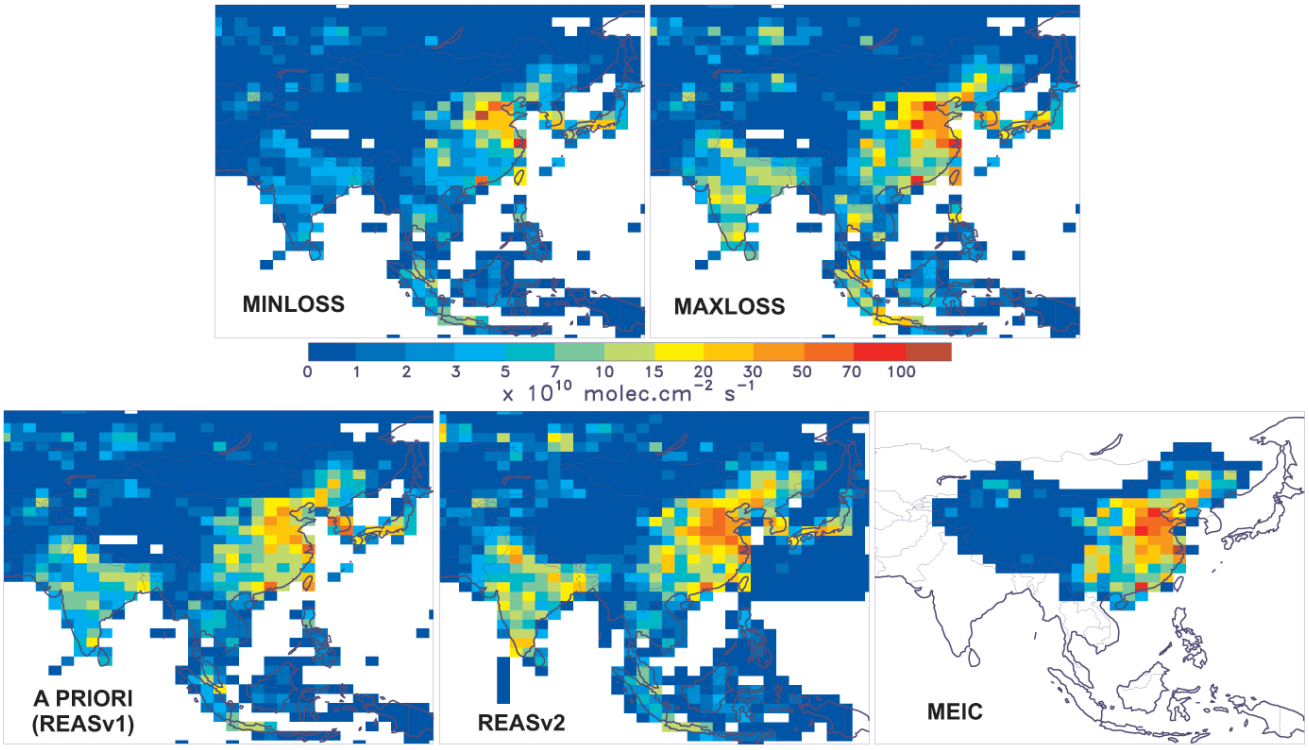

Fig. 13. Comparison between annual anthropogenic emissions inferred from MINLOSS and MAXLOSS inversions (upper panels), and a priori emissions from REASv1, REASv2, and emissions from Multi-Resolution Emission Inventory in China (MEIC) in 2007.

1. Including the reaction $NO+HO_2 \rightarrow HNO_3$ in the model leads to NO_x column decreases estimated at ca. 60 % in oceanic regions and at 30 % over the continental Tropics, whereas the tropospheric NO_x lifetime is reduced globally by 32 %, and the lifetime of methane is decreased by 2.5 yr. Even larger impacts are obtained when adopting the same temperature- and pressure-dependence of the H_2O-assisted rate as in the study of Gottschaldt et al. (2013).

2. The use of laboratory-based rates for the uptake of N_2O_5 by aerosols, instead of the low value suggested by field data, is found to enhance the total NO_x column sink by almost 70 % during winter at mid- and at high latitudes. However, this uncertainty is of little consequence for the comparison of model columns with satellite data obtained around midday local time.

3. The model sensitivity to the rate constant of the NO_2+OH reaction is found to be relatively weak. Compared to a simulation which uses a rate expression constrained by field data (Henderson et al., 2012), the use of the JPL recommendation (Sander et al., 2011) results in a global decrease of NO_x lifetime by 11 %. Furthermore, the influence of OH recycling in isoprene oxidation, as represented in the MIM2+ mechanism, is found to be small on the global scale, although it leads to increased (by up to 20 %) loss rates over remote forested environments.

4. The uptake of HO_2 by fine mode aerosols is found to be the largest source of uncertainty over China, with NO_2 column differences reaching 35 % in winter and 20 % in summer, but also over Europe and the United States in summer, and especially over South Asia during the winter, where the efficient uptake scenario increases NO_2 columns by up to 50 %. The calculated impacts on HO_x species are consistent with the study of Mao et al. (2013) in spite of our neglect of HO_2 uptake on dry or coarse mode aerosols.

The consequences of those sink uncertainties on top-down emissions are explored through emission inversion using model settings which either minimise (MINLOSS) or maximise (MAXLOSS) the total sink. Top-down flux estimates for 2007 are obtained from OMI DOMINO v2 NO_2 columns using the IMAGESv2 model and its adjoint.

Major differences are inferred in the NO_x sources derived in both inversions, by virtue of their substantial differences in NO_x loss rates. More specifically, the global NO_x flux from the MAXLOSS inversion is by almost 80 % higher than in MINLOSS. The largest discrepancies are deduced for soil NO and lightning fluxes (about a factor of two) as well as for anthropogenic emissions in South Asia (factor of 2.4),

reflecting the large sink uncertainties in tropical regions. The global anthropogenic source exhibits somewhat weaker differences, 22 vs. 35 Tg N yr^{-1}.

Between the two inversions, MAXLOSS realises by far the best match with two new anthropogenic inventories for China (REASv2 and MEIC), both in terms of total emission (underestimation by 20–30 % in MAXLOSS, by almost a factor of 2 in MINLOSS) and in terms of spatiotemporal correlation (0.92 for MAXLOSS, 0.75–0.80 for MINLOSS). Over Europe and North America, the choice of the scenario has a large impact on the top-down flux estimates, and results in either lower or higher emissions than in the a priori. Comparisons with INTEX-A and INTEX-B aircraft measurements suggest that the MINLOSS scenario provides the best match with observations both over continents and over ocean, thereby (i) comforting the NO_2+OH rate expression recommended by Henderson et al. (2012), which was also based on INTEX-A data analysis, and (ii) indicating that the formation of HNO_3 in NO+HO_2 might be slower than proposed by Butkovskaya et al. (2009). Note that the latter process was neglected by Henderson et al. (2012) in their Bayesian inversion of rates based on aircraft data; had it been taken into account, an even lower rate constant would have been derived for NO_2+OH in upper tropospheric conditions.

Neither optimization scenario succeeds in improving the agreement with all independent datasets. Whereas comparisons with aircraft measurements and SCIAMACHY data point to MINLOSS as the most likely scenario, an opposite conclusion could be drawn from our analysis of top-down emissions over China. Reasons for this apparent contradiction might be multiple. It should be first pointed out that the formation of HNO_3 in NO+HO_2 has very little influence on NO_x sink rates over China; results essentially similar to those of MAXLOSS would have been obtained if this process had been completely neglected. Secondly, the main reason for the very low Chinese emissions in MINLOSS is the very efficient HO_2 uptake adopted in that scenario. This process has comparatively much less influence in North America, especially in summer, and is therefore not well constrained by INTEX-A and INTEX-B. The poor agreement of MINLOSS with the Chinese inventories might therefore reflect an overestimation of HO_2 uptake on Cu-doped aqueous aerosols, as also suggested by laboratory studies; furthermore, the uptake on organic aerosols (which make up a large fraction of the aerosol surface area over polluted continental regions) might be inhibited in cold or dry conditions (Mikhailov et al., 2009; Virtanen et al., 2010) due to physical changes, more precisely the appearance of a semi-solid or very viscous amorphous state affecting hygroscopic growth and the uptake of radicals. The fact that OH radical levels are strongly underestimated by models in large Chinese cities during summer (Hofzumahaus et al., 2009; Lu et al., 2013) is another indication that the sinks of HO_x might be too strong in the MINLOSS scenario. However, other error sources may bring additional uncertainties. For example, still unknown mechanisms affecting NMVOC oxidation and HONO emissions and/or heterogeneous formation could also contribute to increase OH levels in polluted areas in summer as well as in winter.

In conclusion, the substantial influence of NO_x sink uncertainties on the satellite-derived fluxes shown by our study raises an important issue, largely overlooked in previous inversion studies. Clearly, more research is needed to constrain the relevant processes which might affect NO_x removal. Among these processes, the nitric acid forming channel in NO+HO_2 and the uptake of HO_2 by aerosols were found to represent the largest sources of uncertainty. In view of their potential importance, confirmation by further experimental studies is urgently needed.

Supplementary material related to this article is available online at http://www.atmos-chem-phys.net/13/9057/2013/acp-13-9057-2013-supplement.pdf.

Acknowledgements. This research was supported by the Belgian Science Policy Office through the SECPEA and A3C PRODEX projects.

Edited by: R. Harley

References

Atkinson, R., Baulch, D. L., Cox, R. A., Crowley, J. N., Hampson, R. F., Hynes, R. G., Jenkin, M. E., Rossi, M. J., and Troe, J.: Evaluated kinetic and photochemical data for atmospheric chemistry: Volume I – gas phase reactions of O_x, HO_x, NO_x and SO_x species, Atmos. Chem. Phys., 4, 1461–1738, doi:10.5194/acp-4-1461-2004, 2004.

Beaver, M. R., Clair, J. M. St., Paulot, F., Spencer, K. M., Crounse, J. D., LaFranchi, B. W., Min, K. E., Pusede, S. E., Wooldridge, P. J., Schade, G. W., Park, C., Cohen, R. C., and Wennberg, P. O.: Importance of biogenic precursors to the budget of organic nitrates: observations of multifunctional organic nitrates by CIMS and TD-LIF during BEARPEX 2009, Atmos. Chem. Phys., 12, 5773–5785, doi:10.5194/acp-12-5773-2012, 2012.

Beirle, S., Huntrieser, H., and Wagner, T.: Direct satellite observation of lightning-produced NO_x, Atmos. Chem. Phys., 10, 10965–10986, doi:10.5194/acp-10-10965-2010, 2010.

Bertram, T. H., Thornton, J. A., Riedel, T. P., Middlebrook, A. M., Bahreini, R., Bates, T. S., Quinn, P. K., and Coffman, D. J.: Direct observations of N_2O_5 reactivity on ambient aerosol particles, Geophys. Res. Lett., 36, L19803, doi:10.1029/2009GL040248, 2009.

Boersma, K. F., Eskes, H. J., and Brinksma, E. J.: Error analysis for tropospheric NO_2 retrieval from space, J. Geophys. Res., 109, D04311, doi:10.1029/2003JD003962, 2004.

Boersma, K. F., Eskes, H. J., Meijer, E. W., and Kelder, H. M.: Estimates of lightning NO_x production from GOME satellite observations, Atmos. Chem. Phys., 5, 2311–2331, doi:10.5194/acp-5-2311-2005, 2005.

Boersma, K. F., Eskes, H. J., Veefkind, J. P., Brinksma, E. J., van der A, R. J., Sneep, M., van den Oord, G. H. J., Levelt, P. F., Stammes, P., Gleason, J. F., and Bucsela, E. J.: Near-real time retrieval of tropospheric NO_2 from OMI, Atmos. Chem. Phys., 7, 2103–2118, doi:10.5194/acp-7-2103-2007, 2007.

Boersma, K. F., Eskes, H. J., Dirksen, R. J., van der A, R. J., Veefkind, J. P., Stammes, P., Huijnen, V., Kleipool, Q. L., Sneep, M., Claas, J., Leitão, J., Richter, A., Zhou, Y., and Brunner, D.: An improved tropospheric NO2 column retrieval algorithm for the Ozone Monitoring Instrument, Atmos. Meas. Tech., 4, 1905–1928, doi:10.5194/amt-4-1905-2011, 2011.

Bond, T. C., Streets, D. G., Yarber, K. F., Nelson, S. M., Woo, J.-H., and Klimont, Z.: A technology-based global inventory of black and organic carbon emissions from combustion, J. Geophys. Res., 109, D14203, doi:10.1029/2003JD003697, 2004.

Brown, S. S., William, P., Dube, W. P., Fuchs, H., Ryerson, T. B., Brock, C. A., Bahreini, R., Middlebrook, A. M., Wollny, A. G., Neuman, J. A., Atlas, E., Roberts, J. M., Osthoff, H. D., Trainer, M., Fehsenfeld, F. C., and Ravishankara, A. R.: Reactive uptake coefficients for N_2O_5 determined from aircraft measurements during the Second Texas Air Quality Study : Comparison to current model parameterizations, J. Geophys. Res., 114, D00F10, doi:10.1029/2008JD011679, 2009.

Browne, E. C. and Cohen, R. C.: Effects of biogenic nitrate chemistry on the NO_x lifetime in remote continental regions, Atmos. Chem. Phys., 12, 11917–11932, doi:10.5194/acp-12-11917-2012, 2012.

Browne, E. C., Perring, A. E., Wooldridge, P. J., Apel, E., Hall, S. R., Huey, L. G., Mao, J., Spencer, K. M., Clair, J. M. St., Weinheimer, A. J., Wisthaler, A., and Cohen, R. C.: Global and regional effects of the photochemistry of $CH_3O_2NO_2$: evidence from ARCTAS, Atmos. Chem. Phys., 11, 4209–4219, doi:10.5194/acp-11-4209-2011, 2011.

Butkovskaya, N. I., Kukui, A., Pouvesle, N., and Le Bras, G.: Formation of Nitric Acid in the Gas-Phase HO_2 + NO Reaction: Effects of Temperature and Water Vapor, J. Phys. Chem. A, 109, 6509–6520, doi:10.1021/jp051534v, 2005.

Butkovskaya, N. I., Kukui, A., and Le Bras, G.: HNO_3 forming channel of the HO_2+NO reaction as a function of pressure and temperature in the ranges of 72–600 Torr and 223–323 K, J. Phys. Chem. A, 111, 9047–9053, 2007.

Butkovskaya, N., Rayez, M.-T., Rayez, J.-C., Kukui, A., and Le Bras, G.: Water vapor effect on the HNO_3 yield in the HO_2 + NO reaction: Experimental and theoretical evidence, J. Phys. Chem. A, 113, 11327–11342, 2009.

Butler, T. M., Taraborrelli, D., Brühl, C., Fischer, H., Harder, H., Martinez, M., Williams, J., Lawrence, M. G., and Lelieveld, J.: Improved simulation of isoprene oxidation chemistry with the ECHAM5/MESSy chemistry-climate model: lessons from the GABRIEL airborne field campaign, Atmos. Chem. Phys., 8, 4529–4546, doi:10.5194/acp-8-4529-2008, 2008.

Cariolle, D., Evans, M. J., Chipperfield, M. P., Butkovskaya, N., Kukui, A., and Le Bras, G.: Impact of the new HNO_3-forming channel of the HO_2+NO reaction on tropospheric HNO_3, NO_x, HO_x and ozone, Atmos. Chem. Phys., 8, 4061–4068, doi:10.5194/acp-8-4061-2008, 2008.

Ceulemans, K., Compernolle, S., and Müller, J.-F.: Parameterising secondary organic aerosol from α-pinene using a detailed oxidation and aerosol formation model, Atmos. Chem. Phys., 12, 5343–5366, doi:10.5194/acp-12-5343-2012, 2012.

Costen, R. C., Tennille, G. M., and Levine, J. S.: Cloud pumping in a one-dimensional model, J. Geophys. Res., 93, 15941–15944, 1988.

Cooper, P. L. and Abbatt, J. P. D.: Heterogeneous interactions of OH and HO_2 radicals with surfaces characteristic of atmospheric particulate matter, J. Phys. Chem., 100, 2249–2254, 1996.

Crounse, J. D., Paulot, F., Kjaergaard, H. G., and Wennberg, P. O.: Peroxy radical isomerisation in the oxidation of isoprene, Phys. Chem. Chem. Phys., 13, 13607–13613, 2011.

Davis, J. M., Bhave, P. V., and Foley, K. M.: Parameterization of N_2O_5 reaction probabilities on the surface of particles containing ammonium, sulfate, and nitrate, Atmos. Chem. Phys., 8, 5295–5311, doi:10.5194/acp-8-5295-2008, 2008.

Donahue, N. M. : Atmospheric chemistry: The reaction that wouldn't quit, Nature Chemistry, 3, 98–99, doi:10.1038/nchem.941, 2011.

Elshorbany, Y. F., Kurtenbach, R., Wiesen, P., Lissi, E., Rubio, M., Villena, G., Gramsch, E., Rickard, A. R., Pilling, M. J., and Kleffmann, J.: Oxidation capacity of the city air of Santiago, Chile, Atmos. Chem. Phys., 9, 2257–2273, doi:10.5194/acp-9-2257-2009, 2009.

Erb, K.-H., Gaube, V., Krausmann, F., Plutzar, C., Bondeau, A., and Haberl, H.: A comprehensive global 5min resolution land-use dataset for the year 2000 consistent with national census data, J. Land Use Science, 2, 191–224, doi:10.1080/17474230701622981, 2007.

Eskes, H., van Velthoven, P., Valks, P., and Kelder, H.: Assimilation of GOME total-ozone satellite observations in a three-dimensional tracer-transport model, Q. J. Roy. Meteor. Soc., 129, 1663–1681, doi:10.1256/qj.02.14, 2003.

Evans, M. J. and Jacob, D. J.: Impact of new laboratory studies of N_2O_5 hydrolysis on global model budgets of tropospheric nitrogen oxides, ozone, and OH, Geophys. Res. Lett., 32, L09813, doi:10.1029/2005GL022469, 2005.

Giannelli, R. A., Gilmore, J. H., Landman, L., Srivastava, S., Beardsley, M., Brzezinski, D., Dolce, G., Koupal, J., Pedelty, J., and Shyu, G.: Sensitivity analysis of MOBILE6.0, EPA Report EPA420-R-02-035, US, Environmental Protection Agency, 2002.

Gottschaldt, K., Voigt, C., Jöckel, P., Righi, M., Deckert, R., and Dietmüller, S.: Global sensitivity of aviation NO_x effects to the HNO_3-forming channel of the HO_2 + NO reaction, Atmos. Chem. Phys., 13, 3003–3025, doi:10.5194/acp-13-3003-2013, 2013.

Heald, C. L., Coe, H., Jimenez, J. L., Weber, R. J., Bahreini, R., Middlebrook, A. M., Russell, L. M., Jolleys, M., Fu, T.-M., Allan, J. D., Bower, K. N., Capes, G., Crosier, J., Morgan, W. T., Robinson, N. H., Williams, P. I., Cubison, M. J., DeCarlo, P. F., and Dunlea, E. J.: Exploring the vertical profile of atmospheric organic aerosol: comparing 17 aircraft field campaigns with a global model, Atmos. Chem. Phys., 11, 12673–12696, doi:10.5194/acp-11-12673-2011, 2011.

Henderson, B. H., Pinder, R. W., Crooks, J., Cohen, R. C., Carlton, A. G., Pye, H. O. T., and Vizuete, W.: Combining Bayesian methods and aircraft observations to constrain the $HO^{\bullet}$+ NO_2 reaction rate, Atmos. Chem. Phys., 12, 653–667, doi:10.5194/acp-12-653-2012, 2012.

Hofzumahaus, A., Rohrer, F., Lu, K., Bohn, B., Brauers, T., Chang, C.-C., Fuchs, H., Holland, F., Kita, K., Kondo, Y., Li, X., Lou, S., Shao, M., Zeng, L., Wahner, A., and Zhang, Y.: Amplified trace gas removal in the troposphere, Science, 324, 1702–1704, 2009.

Hudman, R. C., Moore, N. E., Mebust, A. K., Martin, R. V., Russell, A. R., Valin, L. C., and Cohen, R. C.: Steps towards a mechanistic model of global soil nitric oxide emissions: implementation and space based-constraints, Atmos. Chem. Phys., 12, 7779–7795, doi:10.5194/acp-12-7779-2012, 2012.

Irie, H., Boersma, K. F., Kanaya, Y., Takashima, H., Pan, X., and Wang, Z. F.: Quantitative bias estimates for tropospheric NO_2 columns retrieved from SCIAMACHY, OMI, and GOME-2 using a common standard for East Asia, Atmos. Meas. Tech., 5, 2403–2411, doi:10.5194/amt-5-2403-2012, 2012.

Jacob, D. J.: Heterogeneous chemistry and tropospheric ozone, Atmos. Environ., 34, 2131–2159, doi:10.1016/S1352-2310(99)00462-8, 2000.

Jaeglé, L., Steinberger, L., Martin, R. V., and Chance, K.: Global partitioning of NO_x sources using satellite observations : Relative roles of fossil fuel combustion, biomass burning and soil emissions, Faraday Discuss., 130, 407–423, 2005.

Jenkin, M. E., Murrells, T. P., and Passant, N. R.: The temporal dependence of ozone precursor rmissions: estimation and application, AEA Technology, Report No. AEAT/R/ENV/0355 Issue 1, 2000.

Jimenez, J. L., Canagaratna, M. R., Donahue, N. M., Prevot, A. S. H., Zhang, Q., Kroll, J. H., DeCarlo, P. F., Allan, J. D., Coe, H., Ng, N. L., Aiken, A. C., Docherty, K. S., Ulbrich, I. M., Grieshop, A. P., Robinson, A. L., Duplissy, J., Smith, J. D., Wilson, K. R., Lanz, V. A., Hueglin, C., Sun, Y. L., Tian, J., Laaksonen, A., Raatikainen, T., Rautiainen, J., Vaattovaara, P., Ehn, M., Kulmala, M., Tomlinson, J. M., Collins, D. R., Cubison, M. J., Dunlea, E. J., Huffman, J. A., Onasch, T. B., Alfarra, M. R., Williams, P. I., Bower, K., Kondo, Y., Schneider, J., Drewnick, F., Borrmann, S., Weimer, S., Demerjian, K., Salcedo, D., Cottrell, L., Griffin, R., Takami, A., Miyoshi, T., Hatakeyama, S., Shimono, A., Sun, J. Y, Zhang, Y. M., Dzepina, K., Kimmel, J. R., Sueper, D., Jayne, J. T., Herndon, S. C., Trimborn, A. M., Williams, L. R., Wood, E. C., Middlebrook, A. M., Kolb, C. E., Baltensperger, U., and Worsnop, D. R.: Evolution of Organic Aerosols in the Atmosphere, Science, 326, 1525–1529, 2009.

Kubistin, D., Harder, H., Martinez, M., Rudolf, M., Sander, R., Bozem, H., Eerdekens, G., Fischer, H., Gurk, C., Klüpfel, T., Königstedt, R., Parchatka, U., Schiller, C. L., Stickler, A., Taraborrelli, D., Williams, J., and Lelieveld, J.: Hydroxyl radicals in the tropical troposphere over the Suriname rainforest: comparison of measurements with the box model MECCA, Atmos. Chem. Phys., 10, 9705–9728, doi:10.5194/acp-10-9705-2010, 2010.

Kurokawa, J., Ohara, T., Morikawa, T., Hanayama, S., Greet, J.-M., Fukui, T., Kawashima, K., and Akimoto, H.: Emissions of air pollutants and greenhouse gases over Asian regions during 2000–2008: Regional Emission inventory in ASia (REAS) version 2, Atmos. Chem. Phys. Discuss., 13, 10049–10123, doi:10.5194/acpd-13-10049-2013, 2013.

Kwan, A. J., Chan, A. W. H., Ng, N. L., Kjaergaard, H. G., Seinfeld, J. H., and Wennberg, P. O.: Peroxy radical chemistry and OH radical production during the NO_3-initiated oxidation of isoprene, Atmos. Chem. Phys., 12, 7499–7515, doi:10.5194/acp-12-7499-2012, 2012.

Lei, Y., Zhang, Q., He, K. B., and Streets, D. G.: Primary anthropogenic aerosol emission trends for China, 1990–2005, Atmos. Chem. Phys., 11, 931–954, doi:10.5194/acp-11-931-2011, 2011a.

Lei, Y., Zhang, Q., Nielson, C. P., and He, K.: An inventory of primary air pollutants and CO_2 emissions from cement production in China, 1990–2020, Atmos. Environ., 55, 147–154, 2011b.

Lelieveld, J., Butler, T. M., Crowley, J. N., Dillon, T. J., Fischer, H., Ganzeveld, L., Harder, H., Lawrence, M. G., Martinez, M., Taraborrelli, D., and Williams, J.: Atmospheric oxidation capacity sustained by a tropical forest, Nature, 452, 737–740, 2008.

Levelt, P. F., Hilsenrath, E., Leppelmeier, G. W., van Den Oord, G. H. J., Bhartia, P. K., Tamminen, J., De Haan, J. F., and Veefkind, P.: Science Objectives of the Ozone Monitoring Instrument, Geosci. Remote Sens., 44, 1199–1208, doi:10.1109/TGRS.2006.872336, 2006.

Lin, J.-T., McElroy, M. B., and Boersma, K. F.: Constraint of anthropogenic NO_x emissions in China from different sectors: a new methodology using multiple satellite retrievals, Atmos. Chem. Phys., 10, 63–78, doi:10.5194/acp-10-63-2010, 2010.

Lin, J.-T., Liu, Z., Zhang, Q., Liu, H., Mao, J., and Zhuang, G.: Modeling uncertainties for tropospheric nitrogen dioxide columns affecting satellite-based inverse modeling of nitrogen oxides emissions, Atmos. Chem. Phys., 12, 12255–12275, doi:10.5194/acp-12-12255-2012, 2012.

Lin, J.-T.: Satellite constraint for emissions of nitrogen oxides from anthropogenic, lightning and soil sources over East China on a high-resolution grid, Atmos. Chem. Phys., 12, 2881–2898, doi:10.5194/acp-12-2881-2012, 2012.

Lu, K. D., Hofzumahaus, A., Holland, F., Bohn, B., Brauers, T., Fuchs, H., Hu, M., Häseler, R., Kita, K., Kondo, Y., Li, X., Lou, S. R., Oebel, A., Shao, M., Zeng, L. M., Wahner, A., Zhu, T., Zhang, Y. H., and Rohrer, F.: Missing OH source in a suburban environment near Beijing: observed and modelled OH and HO_2 concentrations in summer 2006, Atmos. Chem. Phys., 13, 1057–1080, doi:10.5194/acp-13-1057-2013, 2013.

Ma, J. Z., Beirle, S., Jin, J. L., Shaiganfar, R., Yan, P., and Wagner, T.: Tropospheric NO_2 vertical column densities over Beijing: results of the first three years of ground-based MAX-DOAS measurements (2008–2011) and satellite validation, Atmos. Chem. Phys., 13, 1547–1567, doi:10.5194/acp-13-1547-2013, 2013.

Mao, J., Fan, S., Jacob, D. J., and Travis, K. R.: Radical loss in the atmosphere from Cu-Fe redox coupling in aerosols, Atmos. Chem. Phys., 13, 509–519, doi:10.5194/acp-13-509-2013, 2013.

Martin, R. V., Sauvage, B., Folkins, I., Sioris, C. E., Boone, C., Bernath, P., and Ziemke, J.: Space-based constraints on the production of nitric acid from lightning, J. Geophys. Res., 112, D09309, doi:10.1029/2006JD007831, 2007.

Matthews, E.: Global vegetation and land use : New high-resolution data bases for climate studies, J. Clim. Appl. Meteor., 22, 474–487, 1983.

Matthews, P., George, I., Whalley, L., Brooks, B., Baeza Romero, M. T., and Heard, D.: Heterogeneous uptake of HO_2 radicals onto submicron atmospheric aerosols, Davis Conference on Atmospheric Chemical Mechanisms (ACM), Davis, Calif., 2012.

McLinden, C. A., Fioletov, V., Boersma, K. F., Krotkov, N., Sioris, C. E., Veefkind, J. P., and Yang, K.: Air quality over the Canadian oil sands: A first assessment using satellite observations,

Geophys. Res. Lett., 39, L04804, doi:10.1029/2011GL050273, 2012.

McNeill, V. F., Patterson, J., Wolfe, G. M., and Thornton, J. A.: The effect of varying levels of surfactant on the reactive uptake of N_2O_5 to aqueous aerosol, Atmos. Chem. Phys., 6, 1635–1644, doi:10.5194/acp-6-1635-2006, 2006.

Metzger, S., Dentener, F., Pandis, S., and Lelieveld, J.: Gas/aerosol partitioning, 1, A computationally efficient model, J. Geophys. Res., 107, 4312, doi:10.1029/2001JD001102, 2002.

Mijling, B. and van der A, R. J.: Using daily satellite observations to estimate emissions of short-lived air pollutants on a mesoscopic scale, J. Geophys. Res., 117, D17302, doi:10.1029/2012JD017817, 2012.

Mikhailov, E., Vlasenko, S., Martin, S. T., Koop, T., and Pöschl, U.: Amorphous and crystalline aerosol particles interacting with water vapor: conceptual framework and experimental evidence for restructuring, phase transitions and kinetic limitations, Atmos. Chem. Phys., 9, 9491–9522, doi:10.5194/acp-9-9491-2009, 2009.

Miyazaki, K., Eskes, H. J., and Sudo, K.: Global NO_x emission estimates derived from an assimilation of OMI tropospheric NO2 columns, Atmos. Chem. Phys., 12, 2263–2288, doi:10.5194/acp-12-2263-2012, 2012a.

Miyazaki, K., Eskes, H. J., Sudo, K., Takigawa, M., van Weele, M., and Boersma, K. F.: Simultaneous assimilation of satellite NO_2, O_3, CO, and HNO_3 data for the analysis of tropospheric chemical composition and emissions, Atmos. Chem. Phys., 12, 9545–9579, doi:10.5194/acp-12-9545-2012, 2012b.

Mollner, A. K., Valluvadasan, S., Feng, L., Sprague, M. K., Okumura, M., Milligan, D. B., Bloss, W. J., Sander, S. P., Martien, P. T., Harley, R. A., McCoy, A. B., and Carter, W. P. L.: Rate of Gas Phase Association of Hydroxyl Radical and Nitrogen Dioxide, Science, 330, 646–649, doi:10.1126/science.1193030, 2010.

Müller, J.-F. and Brasseur, G. P.: A three-dimensional chemical transport model of the global troposphere, J. Geophys. Res., 100, 16445–16490, 1995.

Müller, J.-F. and Stavrakou, T.: Inversion of CO and NO_x emissions using the adjoint of the IMAGES model, Atmos. Chem. Phys., 5, 1157–1186, doi:10.5194/acp-5-1157-2005, 2005.

Müller, J.-F., Stavrakou, T., Wallens, S., De Smedt, I., Van Roozendael, M., Potosnak, M. J., Rinne, J., Munger, B., Goldstein, A., and Guenther, A. B.: Global isoprene emissions estimated using MEGAN, ECMWF analyses and a detailed canopy environment model, Atmos. Chem. Phys., 8, 1329–1341, doi:10.5194/acp-8-1329-2008, 2008.

Murray, L. T., Jacob, D. J., Logan, J. A., Hudman, R. C., and Koshak, W. J.: Optimized regional and interannual variability of lightning in a global chemical transport model constrained by LIS/OTD satellite data, J. Geophys. Res., 117, D20307, doi:10.1029/2012JD017934, 2012.

Ohara, T., Akimoto, H., Kurokawa, J., Horii, N., Yamaji, K., Yan, X., and Hayasaka, T.: An Asian emission inventory of anthropogenic emission sources for the period 1980–2020, Atmos. Chem. Phys., 7, 4419–4444, doi:10.5194/acp-7-4419-2007, 2007.

Paulot, F., Crounse, J. D., Kjaergaard, H. G., Kroll, J. H., Seinfeld, J. H., and Wennberg, P. O.: Isoprene photooxidation: new insights into the production of acids and organic nitrates, Atmos. Chem. Phys., 9, 1479–1501, doi:10.5194/acp-9-1479-2009, 2009.

Paulot, F., Henze, D. K., and Wennberg, P. O.: Impact of the isoprene photochemical cascade on tropical ozone, Atmos. Chem. Phys., 12, 1307–1325, doi:10.5194/acp-12-1307-2012, 2012.

Peeters, J. and Müller, J.-F.: HO_x radical regeneration in isoprene oxidation via peroxy radical isomerisations. II: Experimental evidence and global impact, Phys. Chem. Chem. Phys., 12, 14227–14235, doi:10.1039/C0CP00811G, 2010.

Peeters, J., Nguyen, T. L., and Vereecken, L.: HO_x radical regeneration in the oxidation of isoprene, Phys. Chem. Chem. Phys., 11, 5935–5939, doi:10.1039/b908511d, 2009.

Pickering, K., Wang, Y., Tao, W.-K., Price, C., and Müller, J.-F.: Vertical distributions of lightning NO_x for use in regional and global chemical transport models, J. Geophys. Res., 103, 31203–31216, 1998.

Price, C. and Rind, D.: What determines the cloud-to-ground lightning fraction in thunderstorms?, Geophys. Res. Lett., 20, 463–466, 1993.

Ren, X., Olson, J. R., Crawford, J. H., Brune, W. H., Mao, J., Long, R. B., Chen, Z., Chen, G., Avery, M. A., Sachse, G. W., Barrick, J. D., and Diskin, G. S., Huey, L. G., Fried, A., Cohen, R. C., Heikes, B., Wennberg, P. O., Singh, H. B., Blake, D. R., and Shetter, R. E.: HO_x chemistry during INTEX-A 2004: Observation, model calculation, and comparison with previous studies, J. Geophys. Res., 113, D05310, doi:10.1029/2007JD009166, 2008.

Sander, S. P., Abbatt, J., Barker, J. R., Burkholder, J. B., Friedl, R. R., Golden, D. M., Huie, R. E., Kolb, C. E., Kurylo, M. J., Moortgat, G. K., Orkin, V. L., and Wine, P. H.: Chemical Kinetics and Photochemical Data for Use in Atmospheric Studies, Evaluation number 17, NASA Panel for data evaluation, JPL Publication 10-6, Jet Propulsion Laboratory, Pasadena, http://jpldataeval.jpl.nasa.gov, 2011.

Sandu, A. and Sander, R.: Technical note: Simulating chemical systems in Fortran90 and Matlab with the Kinetic PreProcessor KPP-2.1, Atmos. Chem. Phys., 6, 187–195, doi:10.5194/acp-6-187-2006, 2006.

Saunders, S. M., Jenkin, M. E., Derwent, R. G., and Pilling, M. J.: Protocol for the development of the Master Chemical Mechanism, MCM v3 (Part A): tropospheric degradation of non-aromatic volatile organic compounds, Atmos. Chem. Phys., 3, 161–180, doi:10.5194/acp-3-161-2003, 2003.

Schultz, M. G., Backman, L., Balkanski, Y., Bjoerndalsaeter, S., Brand, R., Burrows, J. P., Dalsoeren, S., de Vasconcelos, M., Grodtmann, B., Hauglustaine, D. A., Heil, A., Hoelzemann, J. J., Isaksen, I. S. A., Kaurola, J., Knorr, W., Ladstaetter-Weißenmayer, A., Mota, B., Oom, D., Pacyna, J., Panasiuk, D., Pereira, J. M. C., Pulles, T., Pyle, J., Rast, S., Richter, A., Savage, N., Schnadt, C., Schulz, M., Spessa, A., Staehelin, J., Sundet, J. K., Szopa, S., Thonicke, K., van het Bolscher, M., van Noije, T., van Velthoven, P., Vik, A. F., and Wittrock, F.: REanalysis of the TROpospheric chemical composition over the past 40 years (RETRO): A long-term global modeling study of tropospheric chemistry, Jülich/Hamburg, Germany, 48/2007 report on Earth System Science of the Max Planck Institute for Meteorology, Hamburg, http://retro.enes.org, ISSN 1614-1199, 2007.

Schumann, U. and Huntrieser, H.: The global lightning-induced nitrogen oxides source, Atmos. Chem. Phys., 7, 3823–3907, doi:10.5194/acp-7-3823-2007, 2007.

Singh, H. B., Brune, W. H., Crawford, J. H., Jacob, D. J., and Russell, P. B.: Overview of the summer 2004 Intercontinental

Chemical Transport Experiment-North America (INTEX-A), J. Geophys. Res., 111, D24S01, doi:10.1029/2006JD007905, 2006.

Singh, H. B., Salas, L., Herlth, D., Kolyer, R., Czech, E., Avery, M., Crawford, J. H., Pierce, R. B., Sachse, G. W., Blake, D. R., Cohen, R. C., Bertram, T. H., Perring, A., Wooldridge, P. J., Dibb, J., Huey, G., Hudman, R. C., Turquety, S., Emmons, L., Flocke, F. M., Tang, Y., Carmichael, G. R., and Horowitz, L. W.: Reactive nitrogen distribution and partitioning in the North American troposphere and lowermost stratosphere, J. Geophys. Res., 112, D12S04, doi:10.1029/2006JD007664, 2007.

Singh, H. B., Brune, W. H., Crawford, J. H., Flocke, F., and Jacob, D. J.: Chemistry and transport of pollution over the Gulf of Mexico and the Pacific: spring 2006 INTEX-B campaign overview and first results, Atmos. Chem. Phys., 9, 2301–2318, doi:10.5194/acp-9-2301-2009, 2009.

Sörgel, M., Regelin, E., Bozem, H., Diesch, J.-M., Drewnick, F., Fischer, H., Harder, H., Held, A., Hosaynali-Beygi, Z., Martinez, M., and Zetzsch, C.: Quantification of the unknown HONO daytime source and its relation to NO_2, Atmos. Chem. Phys., 11, 10433–10447, doi:10.5194/acp-11-10433-2011, 2011.

Søvde, O. A., Hoyle, C. R., Myhre, G., and Isaksen, I. S. A.: The HNO_3 forming branch of the HO_2 + NO reaction: pre-industrial-to-present trends in atmospheric species and radiative forcings, Atmos. Chem. Phys., 11, 8929–8943, doi:10.5194/acp-11-8929-2011, 2011.

Spracklen, D. V., Jimenez, J. L., Carslaw, K. S., Worsnop, D. R., Evans, M. J., Mann, G. W., Zhang, Q., Canagaratna, M. R., Allan, J., Coe, H., McFiggans, G., Rap, A., and Forster, P.: Aerosol mass spectrometer constraint on the global secondary organic aerosol budget, Atmos. Chem. Phys., 11, 12109–12136, doi:10.5194/acp-11-12109-2011, 2011.

Stavrakou, T. and Müller, J.-F.: Grid-based versus big region approach for inverting CO emissions using Measurement of Pollution in the Troposphere (MOPITT) data, J. Geophys. Res., 111, D15304, doi:10.1029/2005JD006896, 2006.

Stavrakou, T., Müller, J.-F., Boersma, K. F., De Smedt, I., and van der A, R. J.: Assessing the distribution and growth rates of NO_x emission sources by inverting a 10-year record of NO_2 satellite columns, Geophys. Res. Lett., 35, L10801, doi:10.1029/2008GL033521, 2008.

Stavrakou, T., Müller, J.-F., De Smedt, I., Van Roozendael, M., van der Werf, G. R., Giglio, L., and Guenther, A.: Evaluating the performance of pyrogenic and biogenic emission inventories against one decade of space-based formaldehyde columns, Atmos. Chem. Phys., 9, 1037–1060, doi:10.5194/acp-9-1037-2009, 2009a.

Stavrakou, T., Müller, J.-F., De Smedt, I., Van Roozendael, M., van der Werf, G. R., Giglio, L., and Guenther, A.: Global emissions of non-methane hydrocarbons deduced from SCIAMACHY formaldehyde columns through 2003–2006, Atmos. Chem. Phys., 9, 3663–3679, doi:10.5194/acp-9-3663-2009, 2009b.

Stavrakou, T., Müller, J.-F., De Smedt, I., Van Roozendael, M., Kanakidou, M., Vrekoussis, M., Wittrock, F., Richter, A., and Burrows, J. P.: The continental source of glyoxal estimated by the synergistic use of spaceborne measurements and inverse modelling, Atmos. Chem. Phys., 9, 8431–8446, doi:10.5194/acp-9-8431-2009, 2009c.

Stavrakou, T., Peeters, J., and Müller, J.-F.: Improved global modelling of HO_x recycling in isoprene oxidation: evaluation against the GABRIEL and INTEX-A aircraft campaign measurements, Atmos. Chem. Phys., 10, 9863–9878, doi:10.5194/acp-10-9863-2010, 2010.

Stavrakou, T., Müller, J.-F., Peeters, J., Razavi, A., Clarisse, L., Clerbaux, C., Coheur, P.-F., Hurtmans, D., De Mazière, M., Vigouroux, C., Deutscher, N. M., Griffith, D. W. T., Jones, N., and Paton-Walsh, C.: Satellite evidence for a large source of formic acid from boreal and tropical forests, Nat. Geosci., 5, 26–30, doi:10.1038/ngeo1354, 2012.

Steinkamp, J. and Lawrence, M. G.: Improvement and evaluation of simulated global biogenic soil NO emissions in an AC-GCM, Atmos. Chem. Phys., 11, 6063–6082, doi:10.5194/acp-11-6063-2011, 2011.

Stone, D., Evans, M. J., Edwards, P. M., Commane, R., Ingham, T., Rickard, A. R., Brookes, D. M., Hopkins, J., Leigh, R. J., Lewis, A. C., Monks, P. S., Oram, D., Reeves, C. E., Stewart, D., and Heard, D. E.: Isoprene oxidation mechanisms: measurements and modelling of OH and HO_2 over a South-East Asian tropical rainforest during the OP3 field campaign, Atmos. Chem. Phys., 11, 6749–6771, doi:10.5194/acp-11-6749-2011, 2011.

Su, H., Cheng, Y. F., Shao, M., Gao, D. F., Yu, Z. Y., Zeng, L. M., Slanina, J., Zhang, Y. H., and Wiedensohler, A.: Nitrous acid (HONO) and its daytime sources at a rural site during the 2004 PRIDE-PRD experiment in China, J. Geophys. Res., 113, D14312, doi:10.1029/2007JD009060, 2008.

Su, H., Cheng, Y., Oswald, R., Behrendt, T., Trebs, I., Meixner, F. X., Andreae, M. O., Cheng, P., Zhang, Y., and Pöschl, U.: Soil nitrite as a source of atmospheric HONO and OH radicals, Science, 333, 1616–1618, 2011.

Taketani, F., Kanaya, Y., and Akimoto, H. : Kinetics of heterogeneous reaction of HO_2 radical at ambient concentration levels with $(NH_4)_2SO_4$ and NaCl aerosol particles, J. Phys. Chem. A, 112, 2370–2377, doi:10.1021/jp0769936, 2008.

Taraborrelli, D., Lawrence, M. G., Butler, T. M., Sander, R., and Lelieveld, J.: Mainz Isoprene Mechanism 2 (MIM2): an isoprene oxidation mechanism for regional and global atmospheric modelling, Atmos. Chem. Phys., 9, 2751–2777, doi:10.5194/acp-9-2751-2009, 2009.

van der Werf, G. R., Randerson, J. T., Giglio, L., Collatz, G. J., Mu, M., Kasibhatla, P. S., Morton, D. C., DeFries, R. S., Jin, Y., and van Leeuwen, T. T.: Global fire emissions and the contribution of deforestation, savanna, forest, agricultural, and peat fires (1997–2009), Atmos. Chem. Phys., 10, 11707–11735, doi:10.5194/acp-10-11707-2010, 2010.

van Noije, T. P. C., Eskes, H. J., Dentener, F. J., Stevenson, D. S., Ellingsen, K., Schultz, M. G., Wild, O., Amann, M., Atherton, C. S., Bergmann, D. J., Bey, I., Boersma, K. F., Butler, T., Cofala, J., Drevet, J., Fiore, A. M., Gauss, M., Hauglustaine, D. A., Horowitz, L. W., Isaksen, I. S. A., Krol, M. C., Lamarque, J.-F., Lawrence, M. G., Martin, R. V., Montanaro, V., Müller, J.-F., Pitari, G., Prather, M. J., Pyle, J. A., Richter, A., Rodriguez, J. M., Savage, N. H., Strahan, S. E., Sudo, K., Szopa, S., and van Roozendael, M.: Multi-model ensemble simulations of tropospheric NO_2 compared with GOME retrievals for the year 2000, Atmos. Chem. Phys., 6, 2943–2979, doi:10.5194/acp-6-2943-2006, 2006.

Virtanen, A., Joutsensaari, J., Koop, T., Kannosto, J., Yli-Pirila, P., Leskinen, J., Makela, J. M., Holopainen, J. K., Pöschl, U., Kulmala, M., Worsnop, D. R., and Laaksonen, A.: An amorphous

solid state of biogenic secondary organic aerosol particles, Nature, 467, 824–827, 2010.

Wang, S. W., Zhang, Q., Streets, D. G., He, K. B., Martin, R. V., Lamsal, L. N., Chen, D., Lei, Y., and Lu, Z.: Growth in NO_x emissions from power plants in China: bottom-up estimates and satellite observations, Atmos. Chem. Phys., 12, 4429–4447, doi:10.5194/acp-12-4429-2012, 2012.

Wesely, M. L.: Parameterization of surface resistance to gaseous dry deposition in regional-scale numerical models, Atmos. Environ., 23, 1293–1304, 1989.

Wiedinmyer, C., Akagi, S. K., Yokelson, R. J., Emmons, L. K., Al-Saadi, J. A., Orlando, J. J., and Soja, A. J.: The Fire INventory from NCAR (FINN): a high resolution global model to estimate the emissions from open burning, Geosci. Model Dev., 4, 625–641, doi:10.5194/gmd-4-625-2011, 2011.

Yienger, J. J. and Levy, H.: Empirical model of global soil-biogenic NO_x emissions, J. Geophys. Res., 100, 11447–11464, 1995.

Yuan, B., Hu, W. W., Shao, M., Wang, M., Chen, W T., Lu, S. H., Zeng, L. M., and Hu, M.: VOC emissions, evolutions and contributions to SOA formation at a receptor site in Eastern China, Atmos. Chem. Phys. Discuss., 13, 6631–6679, doi:10.5194/acpd-13-6631-2013, 2013.

Zhang, Q., Streets, D. G., He, K., Wang, Y., Richter, A., Burrows, J. P., Uno, I., Jang, C. J., Chen, D., Yao, Z., and Lei, Y.: NO_x emission trends for China, 1995–2004: The view from the ground and the view from space, J. Geophys. Res., 112, D22306, doi:10.1029/2007JD008684, 2007.

Zhang, Q., Streets, D. G., Carmichael, G. R., He, K. B., Huo, H., Kannari, A., Klimont, Z., Park, I. S., Reddy, S., Fu, J. S., Chen, D., Duan, L., Lei, Y., Wang, L. T., and Yao, Z. L.: Asian emissions in 2006 for the NASA INTEX-B mission, Atmos. Chem. Phys., 9, 5131–5153, doi:10.5194/acp-9-5131-2009, 2009.

Zhao, C. and Wang, Y.: Assimilated inversion of NO_x emissions over east Asia using OMI NO_2 column measurements, Geophys. Res. Lett., 36, L06805, doi:10.1029/2008GL037123, 2009.

Zhou, X., Zhang, N., TerAvest, M., Tang, D., Hou, J., Bertman, S., Alaghmand, M., Shepson, P. B., Carroll, M. A., Griffith, S., Dusanter, S., and Stevens, P. S.: Nitric acid photolysis on forest canopy surface as a source for tropospheric nitrous acid, Nat. Geosci., 4, 440–443, doi:10.1038/ngeo1164, 2011.